MODELING OF CRACK PROPAGATION IN A PREMOLAR TOOTH USING FINITE ELEMENT METHOD

Maryam Ramezani

FEDERAL UNIVERSITY OF MINAS GERAIS (UFMG)

SCHOOL OF ENGINEERING

GRADUATE PROGRAM IN STRUCTURAL ENGINEERING

Modeling of Crack Propagation in a Premolar Tooth using Finite Element Method

Author: **Maryam Ramezani**

A thesis submitted to the Department of Structural Engineering of Universidade Federal de Minas Gerais (UFMG) in partial fulfillment of the requirements for the degree of Master of Science in Structural Engineering.

Adviser: **Prof. Dr. Estevam Barbosa de Las Casas**

Co-adviser: **Prof. Dr. Osvaldo Luis Manzoli**

Examination committee:

Prof. Dr. Estevam Barbosa de Las Casas
DEES – UFMG (Adviser)

Prof. Dr. Osvaldo Luis Manzoli
FEB – UNESP (Co-adviser)

Prof. Dr. Felicio Bruzzi Barros
DEES – UFMG (Internal Examiner)

Profa. Dr. Cláudia Machado de Almeida Mattos
UFES (External Examiner)

Belo Horizonte, Brazil

October 2017

Ramezani, Maryam.
R172m Modeling of crack propagation in a premolar tooth using finite element method [manuscrito] / Maryam Ramezani. - 2017.
vii, 46 f.enc.: il.

Orientador: Estevam Barbosa de Las Casas.
Coorientador: Osvaldo Luis Manzoli.

Tese (doutorado) Universidade Federal de Minas Gerais, Escola de Engenharia.

Bibliografia: f. 43-46.

1. Engenharia de estruturas - Teses. 2. Biomecânica - Teses. 3. Dentes - Teses. 4. Bicúspides - Teses. 5. Método dos elementos finitos - Teses. I. Las Casas, Estevam Barbosa de. II. Manzoli, Osvaldo Luis. III. Universidade Federal de Minas Gerais. Escola de Engenharia. IV. Título.

CDU: 624(043)

ABSTRACT

The term cracked tooth syndrome refers to an incomplete fracture of a vital posterior tooth that involves the dentine and occasionally extends into the pulp. To better understand the characteristics of the cracked tooth syndrome, a cracked premolar tooth will be studied here by using computational techniques. The first step for the analysis is the development of a 3D geometric model to serve as the basis for a finite element analysis. This model, generated from a commercial code, will be exported to a crack propagation program. By having the 3D model and choosing an appropriate crack propagation technique that fits the problem, one can define the material properties and loading types and conduct the crack propagation procedure under various loading conditions. A 2D model is fully studied while some initial results are extracted for the 3D model. Finally, the numerically obtained results can be compared with clinical results obtained from the literature.

Keywords: *Finite element method, crack propagation, premolar tooth, Biomechanical engineering*

RESUMO

O termo síndrome do dente rachado refere-se a uma fratura incompleta de um dente posterior vital que envolve a dentina e ocasionalmente se estende para a polpa. Para entender melhor as características da síndrome do dente rachado, um dente pré-molar rachado será estudado aqui usando técnicas computacionais. O primeiro passo para a análise é o desenvolvimento de um modelo geométrico 3D para servir como base para uma análise de elementos finitos. Este modelo, gerado a partir de um código comercial, será exportado para um programa de propagação de fissura. Ao ter o modelo 3D e escolher uma técnica apropriada de propagação de fissuras que se encaixa no problema, pode-se definir as propriedades do material e os tipos de carga e realizar o processo de propagação de fissuras em várias condições de carga. Um modelo 2D é totalmente estudado enquanto alguns resultados iniciais são extraídos para o modelo 3D. Finalmente, os resultados obtidos numericamente podem ser comparados com os resultados clínicos obtidos a partir da literatura.

Palavras-chave: *Método dos elementos finitos, Propagação de fissuras, Dente pré-molar, Engenharia biomecânica*

ACKNOWLEDGMENT

To my parents and my brother for their kindness and encouragement in all journeys of my life. A very special thanks to my lovely husband *Mohammad*, for his unconditional love that always support me to overcome everything I am facing. I could have never imagined myself where I am at this moment without their endless support.

I would like to thank my adviser Prof. Dr. Estevam Barbosa de Las Casas for giving me the opportunity to work with him as an MSc student and guided me to learn too many new things in the field of biomechanics. I also appreciate the guidance from my co-adviser Prof. Dr. Osvaldo Luis Manzoli for giving me a chance to work with his code and perform the whole analyses under his support. In addition, I would like to thank my Master committee members, Profa. Dr. Cláudia Machado de Almeida Mattos and Prof. Dr. Felicio Bruzzi Barros for their constructive comments to have this final version of my thesis.

To the members of the MECBIO laboratory in DEEs-UFMG, especially Veronika, and Prof. Osvaldo's group members, specifically Eduardo. I wish you all the best in your future. I also gratefully acknowledge the fully and partially financial supports from the Brazilian research agencies CAPES (Coordination for the Improvement of Higher Education Personnel), CNPq (National Council for Scientific and Technological Developments) and FAPEMIG (Research Support Foundation of the State of Minas Gerais).

To my parents and my beloved husband.

Table of Contents

LIST OF FIGURES

LIST OF TABLES

CHAPTER 1 - INTRODUCTION

1.1 Cracked Tooth Syndrome

The term cracked tooth syndrome (CTS) refers to an incomplete fracture of a vital posterior tooth that involves the dentine and occasionally extends into the pulp (Cameron, 1964; Rosen, 1982; Lynch et al, 2002). The symptoms are very variable, making it a notoriously difficult condition to diagnose. The term was first introduced by Cameron in 1964 (Cameron, 1964), who noted a correlation between restoration size and the occurrence of CTS. It was mentioned in the earlier literature of pulpal pain resulting from incomplete tooth fractures. A more recent attempt to define the nature of this condition describes it "*as a fracture plane of unknown depth and direction passing through tooth structure that may progress to communicate with the pulp and/or periodontal ligament*" (Ellis, 2001). The condition presents mainly in patients aged between 30 years and 50 years (Hiatt, 1973; Snyder, 1976; Ellis et al, 1999). Men and women are equally affected (Türp et al, 1996). Mandibular second molars, followed by mandibular first molars and maxillary premolars, are the most commonly affected teeth (Rosen, 1982; Braly et al, 1981). Two classic patterns of crack formation exist. The first occurs when the crack is centrally located; the second is where the crack is more peripherally directed and may result in cuspal fracture. Pressure applied to the crown of a cracked tooth leads to separation of the tooth components along the line of the crack and causes pain.

1.2 Literature Survey

Teeth with or without restorations may exhibit CTS problem, but teeth restored with typical silver alloy restorations are most susceptible. Figure 1.1 shows different types of cracked teeth.

Figure 1.1. Different types of cracked teeth (Internet, 2016)

There are different clinical studies during last decades dedicated to fracture analysis of teeth under various conditions, from restored to root canal treated tooth. Siso et al. (2007) compared the cusp fracture resistance of teeth restored with composite resins. They concluded that, for root filled maxillary premolars, adhesive resin composite restorations increased the fracture resistance of the buccal cusps. Goldberg et al. (2009) investigated the restoration of endodontically treated teeth and concluded that a ferrule of 1-2 mm of tooth tissue coronal to the finish line of the crown significantly improves the fracture resistance of the tooth and is more important than the type of the material of the core and post.

Symptomatic, incompletely fractured posterior teeth can be a great source of anxiety for both patient and dental operator. For the latter, there are some challenges associated with deriving the correct diagnosis with an efficient and time management of cracked tooth syndrome cases. Banerji et al. (2010a) discussed in detail the background of this syndrome including its epidemiology and diagnosis, along with various considerations related to the CTS syndrome.

Banerji et al. (2010b) focused on the immediate and intermediate management, and provided a definition for them, of cracked teeth, and also provided a detailed account of the application of both direct and indirect restorations and restorative techniques used respectively in the management of teeth affected by this complex syndrome. They concluded that "direct restorations with cuspal coverage, in particular bonded composite restorations appear to be the most beneficial when considering prognostic outcome of teeth restored for the purposes of incomplete posterior tooth fractures" (Banerji et al, 2010b).

A review of the literature to establish what evidence exists regarding the risk factors for cracked teeth and their prevention, diagnosis, and treatment was made by Lubisich et al. (2010). They found in the literature that almost all cracks are located in posterior teeth especially in mandibular molar. The risk factors for a cracked tooth are multifactorial: natural causes (i.e. tooth form, age, and wear patterns) or iatrogenic causes (i.e., tooth preparation). More controlled clinical studies are needed to determine which treatment modalities are best suited for specific clinical situations. Recent research has shown that cracks in teeth with no restorations, as well as fractures in the maxillary molars, appear more frequently than once thought. Table 1.1 summarizes the data on the proportion of cracked teeth by tooth type reported from 12 studies. This Table also shows the percentages of maxillary and mandibular molars and premolars with cracks as well as the total number of teeth in the study with cracks and/or

fractures. Averaging the results of the 12 studies investigated in (Lubisich et al., 2010) shows that once a tooth is found to have a crack, 48% of cracked teeth are mandibular molars, 28% are maxillary molars, 16% are maxillary premolars, 6% are mandibular premolars, and about 2% are other teeth.

Table 1.1. Proportion of cracked teeth by tooth type from 12 clinical studies (Lubisich et al., 2010)

Study author	Tooth type	Incidence rate (%)	Total teeth	% unrestored
Cameron (1964)	Mandibular molars	54	50	---
	Maxillary molars	28		
	Mandibular premolars	2		
	Maxillary premolars	16		
	Other	0		
Hiatt (1973)	Mandibular molars	70	100	35
	Maxillary molars	19		
	Mandibular premolars	10		
	Maxillary premolars	1		
	Other	0		
Talim and Gohil (1974)	Mandibular molars	45	---	---
	Maxillary molars	22.5		
	Mandibular premolars	7.5		
	Maxillary premolars	25		
	Other	0		
Cameron (1976)	Mandibular molars	66.7	102	---
	Maxillary molars	23.5		
	Mandibular premolars	0		
	Maxillary premolars	9.8		
	Other	0		
Abou-Rass (1983)	Mandibular molars	45.8	120	15.8
	Maxillary molars	20.8		
	Mandibular premolars	0		
	Maxillary premolars	19.2		
	Other	14.2		
Cavel et al. (1985)	Mandibular molars	44.9	118	4.2
	Maxillary molars	25.4		
	Mandibular premolars	5.1		

	Maxillary premolars	24.6		
	Other	0		
Eakle et al. (1986)	Mandibular molars	43.2	206	8.7
	Maxillary molars	25.73		
	Mandibular premolars	25.24		
	Maxillary premolars	5.83		
	Other	0		
Lagouvardos et al. (1989)	Mandibular molars	46.5	200	---
	Maxillary molars	20		
	Mandibular premolars	5		
	Maxillary premolars	28.5		
	Other	0		
Bader et al. (2001)	Mandibular molars	36.3	377	---
	Maxillary molars	22		
	Mandibular premolars	6.9		
	Maxillary premolars	20.4		
	Other	14.3		
Brynjulfsen et al. (2002)	Mandibular molars	28.3	46	---
	Maxillary molars	39.1		
	Mandibular premolars	4.3		
	Maxillary premolars	28.3		
	Other	0		
Roh et al. (2006)	Mandibular molars	36.4	154	---
	Maxillary molars	57.1		
	Mandibular premolars	1.9		
	Maxillary premolars	4.6		
	Other	0		
Krell and Rivera (2007)	Mandibular molars	59.6	796	---
	Maxillary molars	29.9		
	Mandibular premolars	1.6		
	Maxillary premolars	8.9		
	Other	0		

Silva et al. (2012) studied and analyzed the effect of different load application devices on fracture resistance and failure mode of maxillary premolars restored with composite resin. They showed that

the type of load application device influences significantly the behavior of the teeth-restoration complex during mechanical fracture resistance test.

Las Casas et al. (2014) presented a numerical predictive analysis of crack propagation which may lead to fracture after root reconstruction. A scalar damage model based on the maximum principal stress criterion was used to predict crack propagation. The parameters of the constitutive model were the elastic properties, the tensile strength and the fracture energy of the material. They have concluded that when weakened roots of endodontically treated teeth are treated with adhesive composite reconstruction and post/core restoration, the risk of tensile damage to the root walls is higher with stronger adhesive interfaces. Apparently, localized failures of the interface corresponding to peak stress areas decrease the risk of damage to the root dentin walls. Lin et al. (2013) presented an investigation of the failure risk for an endodontically treated restored premolar. They considered different crack depths along with three different computer-aided design procedures. In addition, the ceramic onlay, endo-crown, and conventional crown restorations are used to simulate the 3D FE models. The results indicated that the stress values on the enamel, dentin, and luting cement for endo-crown restorations exhibited the lowest values relative to the other two restoration methods.

The enamel of human teeth is generally regarded as a brittle material with low fracture toughness. Consequently, the contributions of this tissue in resisting tooth fracture and the importance of its complex have been largely overlooked. Experimental analysis of the tooth microstructure was done by Yahyazadehfar et al. (2013) . Based on their analyses, they concluded that the fracture resistance of enamel is both inhomogeneous and spatially anisotropic. The cracks initiating at the surface of teeth may begin extension towards the dentin–enamel junction. They are deflected by the decussated rods and continue growth about the tooth periphery, transverse to the rods in the outer enamel. This process helps the dissipation of fracture energy and prevents cracks from propagating towards the dentin and vital pulp.

Yahyazadehfar et al. (2014) studied the complex microstructures of tooth tissues, their roles in resisting tooth fracture and the importance of hydration and aging on the fracture resistance of tooth tissues is discussed. Their results show that both enamel and dentin are primarily extrinsically toughened and it arises from the development of unbroken ligaments that act to shield the crack through the development of bridging stresses. Finally, they concluded that the extrinsic toughening plays a critical role in the fatigue crack growth resistance of dentin and enamel, and also the crack growth

resistance of these materials is considerably lower under cyclic conditions in comparison to that in quasi static loading.

Munari et al. (2015) studied and compared the areas of stress concentration in a 3D premolar tooth model with anisotropic or isotropic enamel using the finite element method. Because tooth structures are more resistant to compression, damage such as the formation of cracks and fracture of tooth structure are likely to be caused by tensile stress from the eccentric contacts of unbalanced occlusion. One of the main conclusion of this study was that the tensile stresses generated by the applications of axial and oblique loads in isotropic models was larger than those in the anisotropic models, but the stress distribution was similar.

Study of the behavior of thin interface regions between distinguished components of composite structural members was conducted by Manzoli et al. (2012) using standard solid finite elements with a very high aspect ratio. It has been shown that these elements present the same kinematics as the continuous strong discontinuity approach. They concluded that their new technique helps users to utilize very thin interfaces in a continuum framework, without the need of mesh refinement in the interface area. In their numerical examples, the proposed damage constitutive model has shown that the response of the continuum damage model becomes similar to the response that would be obtained with a discrete relation.

Manzoli et al. (2016) used a new technique called "mesh fragmentation" for modelling cracks in quasi-brittle materials based on the use of interface solid finite elements. "*A tension damage constitutive relation between stresses and strains is proposed to describe crack formation and propagation. The constitutive model is integrated using an implicit-explicit integration scheme to avoid convergence drawbacks, commonly found in problems involving discontinuities*". The results show that the technique is able to predict satisfactorily the behavior of structural members involving different crack patterns, including multiple cracks, without significant mesh dependency provided that unstructured meshes are used.

In addition, there are various investigation reporting the loading magnitude for a tooth under different loading conditions. Here are a summaries on the load values considered in various investigations: a maximum load of 522 N was proposed in (Lyons et al, 1996; Proeschel et al, 2002) using the experimental techniques; a FE study on a mandibular premolar tooth with a loading of 400

N was conducted in (Palamara et al, 2002); a maximum biting force of 453 N was reported in (Litonjua et al, 2004) based on experimental evaluation technique; a load of 380 N was applied on an implanted premolar tooth (Hisam et al, 2015); and, a maximum load of 600 N was considered in (Misch, 2015) applied on premolar tooth.

1.3 Motivation and Objectives

Finite Element Method (FEM) has been widely used for the numerical modeling of structural problems (Hughes, 2000; Zienkiewicz et al, 2005). With the advent and popularization of high-performance computers, the FEM is gaining more space in dental related applications over the past two decades. Furthermore, improving the performance of the finite elements has been, in recent years, important objects of studies and discussions. The use of computer-based FEM programs was greatly facilitated with the development of pre- and post-processors rich interactive graphics capabilities, allowing users with basic knowledge of geometry to easily work with them. On the other hand, there are phenomena which performs the conventional form of the FEM cannot satisfactorily describe, raising the development of new strategies for this purpose. Problems subjected to large deformation and crack propagation, which require several changes in the discretization of the structure (remeshing), are among those responsible to arise the interest for these new developments. The main focus of early implementations of Finite Element (FE) models for discontinuity problems was defining meshes conformed to discontinuity surfaces (Ingraea et al, 1985; Swenson et al, 1988). Not only generating a mesh compatible with discontinuity surfaces is a challenging task in developing the finite element models, but computed solutions of such models may also suffer from inaccuracy and mesh-dependency. Moreover, redefining the mesh to capture the solution is inevitable for evolving discontinuities. The remeshing becomes cumbersome, time consuming and a computationally demanding task especially for three-dimensional problems.

Therefore, the *mesh fragmentation technique* proposed by Manzoli et al. (2016) is considered here to overcome the associated problems with the finite element modeling.

There is a limited number of publications where the researchers tried to model crack growth in teeth using the finite element method. Thus, one can obtain a realistic 3D model of a tooth and study the crack propagation under various conditions. The modeling technique can be chosen from various computational techniques which are available nowadays in the engineering research communities. The

motivation and final goal of this project are "*to predict the crack propagation in tooth structure using a finite element analysis and special crack propagation techniques, as proposed by Manzoli et al. (2016)*".

1.4 Thesis outline

The remainder of the present text is organized as follows:

- **Chapter 2:** Presents an overview of quasi-brittle fracture mechanics formulations. It explains some basic formulations on linear elastic fracture mechanics and relevant texts on quasi-brittle materials;
- **Chapter 3:** Provides the modeling technique and procedure and also some initial results obtained by ABAQUS®;
- **Chapter 4:** Presents the whole analysis methodology in detail, including the whole steps for fracture analysis using the mesh fragmentation technique;
- **Chapter 5:** Presents the results of fracture analysis of the premolar tooth using the mesh fragmentation technique;
- **Chapter 6:** Final chapter is devoted to conclusion and bring the main aspects of this dissertation along with some suggestions for the future researches.

CHAPTER 2- QUASI-BRITTLE FRACTURE

This chapter is devoted to damage and fracture micromechanisms operating in the case when monotonically increasing forces are applied to engineering materials and components. According to the amount of plastic deformation involved in these processes, fracture events can be categorized as brittle, quasi-brittle or ductile.

Brittle fracture is typical for ceramic materials, where plastic deformation is strongly limited across extended ranges of deformation rates and temperatures. In amorphous ceramics, it is simply because of a lack of any dislocations and, simultaneously, strong covalent and ionic interatomic bonds. Metallic materials or polymers exhibit brittle fracture only under conditions of extremely high deformation rates, very low temperatures or extreme impurity concentrations at grain boundaries (Pokluda et al, 2010). In the case of a strong corrosion assistance, brittle fracture can also occur at very small loading rates or even at a constant loading (stress corrosion cracking).

Prior to cracking, quasi-brittle materials like concrete can, for many purposes, be modelled sufficiently accurately as isotropic, linear-elastic. For instance, in a two-dimensional state of stress:

$$\begin{bmatrix}\sigma_{xx}\\ \sigma_{yy}\\ \sigma_{xy}\end{bmatrix} = \frac{E}{1-\nu^2}\begin{bmatrix}1 & \nu & 0\\ \nu & 1 & 0\\ 0 & 0 & 1/2(1-\nu)\end{bmatrix}\begin{bmatrix}\varepsilon_{xx}\\ \varepsilon_{yy}\\ \gamma_{xy}\end{bmatrix} \tag{2-1}$$

where σ_{xx}, σ_{yy}, and σ_{xy} are normal stresses in *x* and *y* directions and shear stress in *xy* plane, respectively; *E* is the Young's modulus; ν is the Poisson ratio; and ε_{xx}, ε_{yy}, and γ_{xy} are strains in *x* and *y* directions, and *xy* plane. When the major principal tensile stress exceeds the tensile strength or, in more generally, when the combination of principal stresses violates a tension cut-off criterion, a crack is initiated perpendicular to the direction of the principal stress. This embodies that in a sampling point, where the stress, strain and history variables are monitored, the isotropic stress-strain relation is replaced by an orthotropic law with the n, *s*-axes the axes of orthotropy, where *n* is the direction normal to the crack and *s* refers to the direction tangential to the crack. In a first attempt the orthotropic relation can be defined as (Rashid, 1968):

$$\begin{bmatrix}\sigma_{nn}\\ \sigma_{ss}\\ \sigma_{ns}\end{bmatrix} = \begin{bmatrix}0 & 0 & 0\\ 0 & E & 0\\ 0 & 0 & 0\end{bmatrix}\begin{bmatrix}\varepsilon_{nn}\\ \varepsilon_{ss}\\ \gamma_{ns}\end{bmatrix} \tag{2-2}$$

where the orthotropic stress-strain relation has been set up in the coordinate system that aligns with the axes of orthotropy. Eq. (2-2) shows that both the normal stiffness and the shear stiffness across the crack are set equal to zero upon cracking. As a consequence, all effects of lateral contraction/expansion also disappear.

If, for a plane-stress situation, $\sigma_{ns} = [\sigma_{nn}, \sigma_{ss}, \sigma_{ns}]^T$ and $\varepsilon_{ns} = [\varepsilon_{nn}, \varepsilon_{ss}, \gamma_{ns}]^T$ the secant stiffness matrix D_{ns}^s is defined as:

$$D_{ns}^s = \begin{bmatrix} 0 & 0 & 0 \\ 0 & E & 0 \\ 0 & 0 & 0 \end{bmatrix} \tag{2-3}$$

one can write the *orthotropic* elastic stiffness relation in the *n*, *s*-coordinate system as:

$$\sigma_{ns} = D_{ns}^s \, \varepsilon_{ns} \tag{2-4}$$

Because of ill-conditioning, use of Eq. (2-2) may result in premature convergence difficulties. Also, physically unrealistic and distorted crack patterns can be obtained, e.g. (Suidan et al, 1973). For this reason a reduced shear modulus βG $(0 \leq \beta \leq 1)$ was reinserted in the model:

$$D_{ns}^s = \begin{bmatrix} 0 & 0 & 0 \\ 0 & E & 0 \\ 0 & 0 & \beta G \end{bmatrix} \tag{2-5}$$

where *G* is the shear modulus. The use of the so-called *shear retention factor* β not only reduces the numerical difficulties, but it also improves the physical reality of fixed crack models, because it can be thought of as a model representation of aggregate interlock. Most researchers simply adopt a constant shear retention factor (β = 0.2 is a commonly adopted value) but sometimes a crack-strain dependent factor is employed (Kolmar et al, 1984). The latter option is more realistic since the capability of a crack to transfer shear stresses in mode-II decreases with increasing crack strain.

The fact that the stiffness normal to the crack in Eq. (2-5) is set equal to zero involves a sudden drop of the *tensile* stress from the initial tensile strength f_t to zero upon crack initiation. Similar to the use of a zero shear retention factor, this may also cause numerical problems. The experimental observation on quasi-brittle materials, like concrete, has led to the replacement of purely brittle crack models by *tension-softening* models, in which a descending branch was introduced to model the gradually diminishing tensile strength of concrete upon further crack opening. In a smeared context, one can model this by inserting a normal reduction factor μ in the secant stiffness matrix:

$$D_{ns}^s = \begin{bmatrix} \mu E & 0 & 0 \\ 0 & E & 0 \\ 0 & 0 & \beta G \end{bmatrix} \tag{2-6}$$

where, similar to the shear reduction factor β, the normal reduction factor μ can be a function of the strain normal to the crack: $\mu = \mu(\varepsilon_{nn})$. A final refinement is given by the addition of Poisson coupling after crack formation. Then, we arrive at the mode-I crack band formulation of Bazant and Oh (1983) extended with mode-II shear retention:

$$D_{ns}^{S}=\begin{bmatrix} \frac{\mu E}{1-\nu^2\mu} & \frac{\nu\mu E}{1-\nu^2\mu} & 0 \\ \frac{\nu\mu E}{1-\nu^2\mu} & \frac{E}{1-\nu^2\mu} & 0 \\ 0 & 0 & \beta G \end{bmatrix} \tag{2-7}$$

A typical micromechanism of brittle fracture is so-called cleavage, where the atoms are gradually separated by tearing along the fracture plane in a very fast way (comparable to the speed of sound). During the last 50 years, the resistance to unstable crack initiation and growth, i.e., the fracture toughness, became a very efficient measure of brittleness or ductility of materials. In the case of cleavage, this quantity can be simply understood in a multiscale context. The continuum linear–elastic fracture mechanics approach were developed by Griffith (1921) and Irwin (1957), brought an important relationship between the crack driving force G_f and the stress intensity factor K_I as:

$$G_f = \frac{1-\nu^2}{E} K_I^2 \tag{2-8}$$

The G_f is defined also as the energy drop related to unit area of a new surface. This relation holds for a straight front of an ideally flat crack under conditions of both the remote mode-I loading and the plane strain. The energy necessary for creation of new fracture surfaces can be supplied from the elastic energy drop of the cracked solid and/or from the work done by external forces (or the drop in the associated potential energy).

CHAPTER 3 – MODELING TECHNIQUE, PROCEDURE AND INITIAL ANALYSES

This chapter gives detailed information on the tooth modeling technique and procedure and also some initial analyses done using commercial code ABAQUS®. It contains the geometry information, material properties, loading types, boundary conditions, and meshing approach.

3.1 Modeling Technique

The main modeling technique comes from the mesh fragmentation procedure proposed by Manzoli et al. (2016), so we just review the whole technique based on this reference. The proposed technique, hereafter called *mesh fragmentation technique*, is based on the use of interface solid finite elements with a high aspect ratio (2012), which are inserted in between standard (bulk) finite elements of a finite element mesh. In this work, these interface elements are responsible for describing the crack formation and propagation via an appropriate continuum damage model.

Figure 1 illustrates the main steps of the proposed mesh fragmentation technique for 2D and 3D problems, which can be summarized as follows:

1. Generation of the standard FE mesh to be fragmented (Figure 3.1 (a)).
2. Separation of the finite elements by introducing gaps in between them (Figure 3.1 (b)).
3. Insertion of interface elements with a high aspect ratio in between the bulk finite elements (Figure 3.1 (c)).

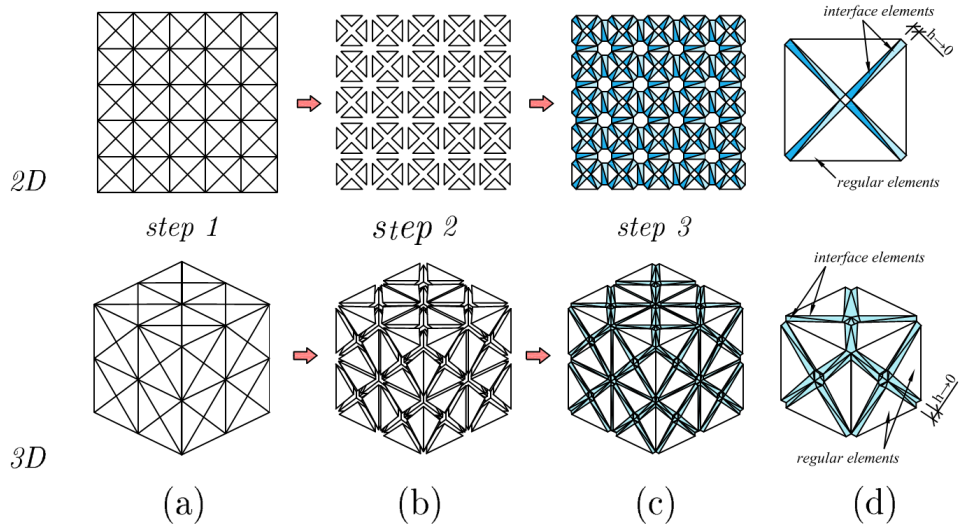

Figure 3.1. 2D and 3D mesh fragmentation process: (a) generation of the standard FE mesh to be fragmented; (b) separation of the finite elements (with an exaggerated scale factor for clarity); (c) insertion of interface elements (depicted in gray); and (d) detail of interface elements between regular elements (Manzoli et al, 2016).

It is important to note in Figure 3.1 (b) that the gaps are in exaggerated scale for illustration. These gaps are usually very small, with a thickness around 1% of the typical size of the regular elements. Therefore, based on Manzoli et al. (2016), the assumption of 1% of the typical size of the regular elements seemed to be a reasonable value, provided that the size of the regular elements has been chosen to accurately capture the (elastic) stress field prior to the crack formation. Triangular/tetrahedron finite elements are used for both the standard FE mesh and the interface elements introduced during the fragmentation process (see Figure 3.1).

With the proposed strategy, cracks can only propagate along the interface elements. For problems in which the region where cracks are expected is known a priori, the mesh fragmentation technique may be applied only in the region of interest. This approach is very attractive since the steps mentioned above are straightforward in implementation, giving place to an additional pre-processing stage. The mesh fragmentation approach is completed by a continuum tension damage model formulated to describe the formation and propagation of cracks along the interfaces.

3.1.1 Interface solid finite element

To describe the main features of the interface solid finite elements in 2D and 3D modeling, standard three-node triangular finite element and four-node tetrahedrons, as illustrated in Figure 3.2, are considered. The geometry of these elements can be characterized by the position of their nodes according to a local Cartesian coordinate system (n, s), defining the unit vector, n, normal to the element base, and the height, h, given by the distance between node 1 and its projection on the element base 1'.

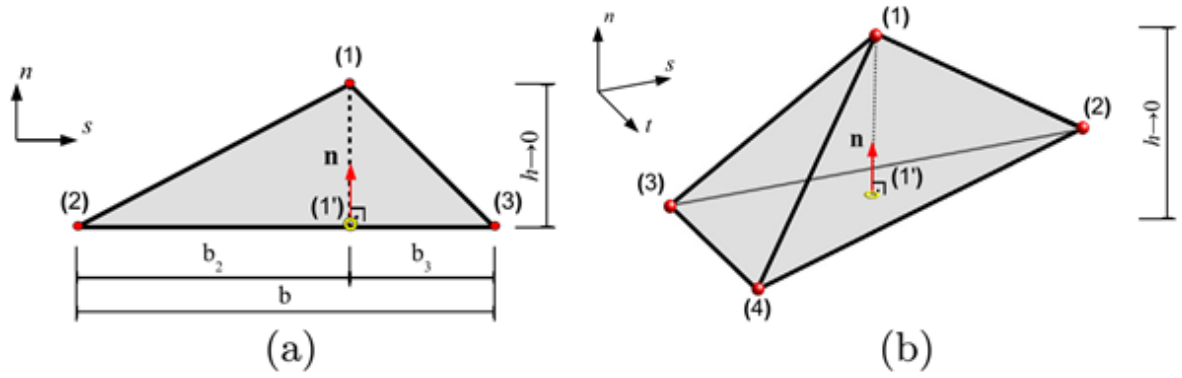

Figure 3.2. Interface solid finite elements: (a) three-node triangular element and (b) four-node tetrahedron element (Manzoli et al, 2016).

Following the standard finite element approximations, the strain field of the solid finite element can be expressed by:

$$\boldsymbol{\varepsilon} = B\boldsymbol{d} \tag{3-1}$$

where B is the strain–displacement matrix and $\boldsymbol{d}$ is the nodal displacement vector of the element.

To show the similarity between the kinematics provided by these elements, when h tends to zero, and that associated to the continuous strong discontinuity approach (CSDA), the strain tensor is divided into two parts (Manzoli et al, 2012):

$$\boldsymbol{\varepsilon} = \tilde{\varepsilon} + \hat{\varepsilon} \tag{3-2}$$

where $\hat{\varepsilon}$ collects all the components of the strain tensor that depends on h, and $\tilde{\varepsilon}$ contains the rest of the components. Thus, the components that depend on h can be written as:

$$\hat{\varepsilon} = \frac{1}{h}(n \otimes [u])^s \tag{3-3}$$

where $(\cdot)^s$ corresponds to the symmetric part of $(\cdot)$, $\otimes$ denotes a dyadic product, and $[u]$ is a vector that collects the components of the relative displacement between node 1 and its projection on the element base 1. The total strain tensor, given by Eq. (3-2), can then be rewritten as:

$$\boldsymbol{\varepsilon} = \tilde{\varepsilon} + \underbrace{\frac{1}{h}(n \otimes [u])^s}_{\hat{\varepsilon}} \tag{3-4}$$

As can be noted from this decomposition, when h tends to zero, the component $\tilde{\varepsilon}$ remains bounded, while the $\hat{\varepsilon}$ component is no longer bounded. As a consequence, in this situation, the element strains are related almost exclusively to the relative displacement between node 1 and its projection on the element base 1'. As described by Manzoli et al. (2012), in the limit situation $(h \to 0)$, the relative displacement $[u]$ becomes the measure of a displacement discontinuity (strong discontinuity), and the structure of the strain field in Eq. (3-4) corresponds to the typical kinematics of the CSDA. Therefore, based on the same concepts of the CSDA, it can be stated that bounded stress can be obtained from unbounded strains by means of a continuum constitutive relation. The equivalence between the strain field of the interface finite elements (when $h \to 0$) and the strong discontinuity kinematics is detailed by Manzoli et al. (2012).

According to the local Cartesian coordinate system (n, s), depicted in Figure 3.2(a), the nodal coordinates of the 3-node triangular finite element are:

$$\begin{aligned} x^{(1)} &= (h, b_2), \\ x^{(2)} &= (0,0), \\ x^{(3)} &= (0, b) \end{aligned} \tag{3-5}$$

Thus, the components of the strain tensor of the element, given by Eq. (3-4), can be expressed as:

$$\tilde{\varepsilon} = \frac{1}{b}\begin{bmatrix} 0 & \frac{1}{2}\left(u_n^{(3)} - u_n^{(2)}\right) \\ \frac{1}{2}\left(u_n^{(3)} - u_n^{(2)}\right) & \left(u_s^{(3)} - u_s^{(2)}\right) \end{bmatrix} \tag{3-6}$$

and

$$\hat{\varepsilon} = \frac{1}{h}\begin{bmatrix} [\![u]\!]_n & \frac{1}{2}[\![u]\!]_s \\ \frac{1}{2}[\![u]\!]_s & 0 \end{bmatrix} \tag{3-7}$$

where $u_n^{(i)}$ and $u_s^{(i)}$ are the components of the displacement of node *i* according to the (n, s) system; while $[\![u]\!]_n = u_n^{(1)} - u_n^{(1')}$ and $[\![u]\!]_s = u_s^{(1)} - u_s^{(1')}$ are the components of the relative displacement $[\![u]\!]$. In the same way, the nodal coordinates of the 4-node tetrahedron finite element (see Figure 3.2(b)) according to a local Cartesian coordinate system (n, s, t):

$x^{(1)} = \left(h, x_s^{(1)}, x_t^{(1)}\right)$,
$x^{(2)} = \left(0, x_s^{(2)}, x_t^{(2)}\right)$,
$x^{(3)} = \left(0, x_s^{(3)}, x_t^{(3)}\right)$,
$x^{(4)} = \left(0, x_s^{(4)}, x_t^{(4)}\right)$.

Thus, the corresponding parts of the strain tensor, given by Eq. (3-4), can be expressed as:

$$\tilde{\varepsilon} = \frac{1}{A}\begin{bmatrix} \tilde{\varepsilon}_{nn} & \tilde{\varepsilon}_{ns} & \tilde{\varepsilon}_{nt} \\ \tilde{\varepsilon}_{ns} & \tilde{\varepsilon}_{ss} & \tilde{\varepsilon}_{st} \\ \tilde{\varepsilon}_{nt} & \tilde{\varepsilon}_{st} & \tilde{\varepsilon}_{tt} \end{bmatrix} \tag{3-8}$$

and

$$\hat{\varepsilon} = \frac{1}{h}\begin{bmatrix} [\![u]\!]_n & \frac{1}{2}[\![u]\!]_s & \frac{1}{2}[\![u]\!]_t \\ \frac{1}{2}[\![u]\!]_s & 0 & 0 \\ \frac{1}{2}[\![u]\!]_t & 0 & 0 \end{bmatrix} \tag{3-9}$$

where

$$\begin{aligned}
\tilde{\varepsilon}_{nn} &= 0, \\
\tilde{\varepsilon}_{ss} &= \frac{1}{2}\left[(x_t^{(3)} - x_t^{(2)})u_s^{(4)} + (x_t^{(2)} - x_t^{(4)})u_s^{(3)} + (x_t^{(4)} - x_t^{(3)})u_s^{(2)}\right], \\
\tilde{\varepsilon}_{tt} &= -\frac{1}{2}\left[(x_s^{(3)} - x_s^{(2)})u_t^{(4)} + (x_s^{(2)} - x_s^{(4)})u_t^{(3)} + (x_s^{(4)} - x_s^{(3)})u_t^{(2)}\right], \\
\tilde{\varepsilon}_{ns} &= \frac{1}{4}\left[(x_t^{(3)} - x_t^{(2)})u_n^{(4)} + (x_t^{(2)} - x_t^{(4)})u_n^{(3)} + (x_t^{(4)} - x_t^{(3)})u_n^{(2)}\right], \\
\tilde{\varepsilon}_{nt} &= -\frac{1}{4}\left[(x_s^{(3)} - x_s^{(2)})u_n^{(4)} + (x_s^{(2)} - x_s^{(4)})u_n^{(3)} + (x_s^{(4)} - x_s^{(3)})u_n^{(2)}\right], \\
\tilde{\varepsilon}_{st} &= \frac{1}{4}\left[(x_t^{(3)} - x_t^{(2)})u_t^{(4)} + (x_t^{(2)} - x_t^{(4)})u_t^{(3)} + (x_t^{(4)} - x_t^{(3)})u_t^{(2)} - (x_s^{(3)}\right. \\
&\qquad \left. - x_s^{(2)})u_s^{(4)} - (x_s^{(2)} - x_s^{(4)})u_s^{(3)} - (x_s^{(4)} - x_s^{(3)})u^{(2)}\right],
\end{aligned} \tag{3-10}$$

A is the area of the element base with unit vector n; $u_n^{(i)}, u_s^{(i)}$ are $u_t^{(i)}$ the components of the displacement of node *1* according to the (n, s, t) system; $[\![u]\!]_n = u_n^{(1)} - u_n^{(1')}$, $[\![u]\!]_s = u_s^{(1)} - u_s^{(1')}$

and $[\![u]\!]_t = u_t^{(1)} - u_t^{(1')}$ are the components of the relative displacement $[\![u]\!]$ between node 1 and the point corresponding to its projection on the element base 1' $\left(x^{(1')} = (0, x_s^{(1)}, x_t^{(1)})\right)$.

3.1.2 Tension damage model

It is known that constitutive models based on the Continuum Damage Mechanics Theory (CDMT) are appropriate to describe the material degradation process due to crack propagation (Kachanov, 1986; Lemaitre, 1992; Cervera et al, 1996; Murakami, 2012;). For this class of models, the mechanical behavior of a damaged material is usually described by using the notion of the effective stress, together with the hypothesis of mechanical equivalence between the damage and the undamaged material.

Here, the phenomenon of crack initiation and propagation through the interface solid finite elements is described by a tension damage model. In the following, the main ingredients of this model and the integration of the stress–strain relation using an implicit–explicit integration scheme are detailed. The resulting discrete relation obtained when the interface element height, *h*, tends to zero is also presented. The tension damage model is defined by the following constitutive relation:

$$\boldsymbol{\sigma} = (1-d)\underbrace{\mathbb{C}:\boldsymbol{\varepsilon}}_{\bar{\sigma}} \tag{3-11}$$

where $\boldsymbol{\sigma}$ is the nominal stress; $d \in [0,1]$ is the scalar damage variable; $\mathbb{C}$ is the fourth order elastic tensor; ε is the strain tensor; and the product $\mathbb{C}:\boldsymbol{\varepsilon}$ defines the effective stress tensor $\bar{\boldsymbol{\sigma}}$. The damage criterion defines the elastic domain and is given by:

$$\phi = \sigma_{nn} - q(r) \leq 0 \tag{3-12}$$

where σ_{nn} is the component of the stress normal to the base of the element ($\sigma_{nn} = \boldsymbol{n}.\boldsymbol{\sigma}.\boldsymbol{n}$), q and r are the stress and strain like internal variables, respectively, and the function $q(r)$ defines the softening law, and ϕ is the damage criterion parameter.

To maintain the stresses bounded when the height tends to zero ($h \to 0$), all components of the displacement jump must tend to zero if $d = 0$ (elastic regime). On the other hand, the damage variable must tend to 1 in the inelastic regime with $[\![u]\!] \neq 0$. Therefore, in the limit situation of $h \to 0$, the interface element presents a rigid-damage behavior. Note that, before the stresses reach the damage criterion all components of the displacement jump are precluded via penalization of $1/h$. This penalization can be seen in the equation of the discrete constitutive model that emerges from the continuum constitutive model. Note that the elastic stiffness of the discrete model is given by the continuum elastic constants (K and G) divided by h, which corresponds to a very high stiffness for very

small values of *h*. This provides a rigid behavior, precluding the evolution of the displacement jump, before the stresses reach the damage criterion.

If the Poisson's ratio is null ($\nu = 0$), the discrete relation can be expressed in terms of the Young's modulus, *E*, since:

$$4G/3 + K = E \text{ and } G = E/2 \tag{3-13}$$

where *G* is the shear modulus and *K* is the bulk modulus. For a monotonic increase (in mode-I) of the normal displacement ($[\![u']\!]_n > 0, [\![u]\!]_s|_{t=0} = 0, [\![u]\!]_s = [\![u]\!]_t = 0$), the evolution of the normal stress becomes:

$$\sigma_{nn}([\![u]\!]_n) = (1-d)\frac{1}{h}E[\![u]\!]_n = \begin{cases} \frac{1}{h}E[\![u]\!]_n & if\ \ [\![u]\!]_n \le [\![u_0]\!]_n \\ (1-d)\frac{1}{h}E[\![u]\!]_n = q(r) & if\ \ [\![u]\!]_n > [\![u_0]\!]_n \end{cases} \tag{3-14}$$

with $[\![u_0]\!]_n = h\, q_0/E$. Assuming an exponential softening law of the form:

$$q(r) = q_0 e^{\mathcal{A}h(1-r/q_0)} \tag{3-15}$$

with $q_0 = f_t$,where f_t is the tensile strength of the material and $\mathcal{A}$ is the softening parameter, the mode-I fracture energy, G_f, i.e., the energy dissipated in a complete degradation of the interface element in mode-I, is given as:

$$G_f = \int_0^{\infty} \sigma_{nn}([\![u]\!]_n) d[\![u]\!]_n = \int_0^{[\![u_0]\!]_n} \sigma_{nn}([\![u]\!]_n) d[\![u]\!]_n \tag{3-16}$$

$$+\int_{[\![u_0]\!]_n}^{\infty} \sigma_{nn}([\![u]\!]_n) d[\![u]\!]_n \tag{3-17}$$

$$G_f = (f_t^2 h/2 + f_t^2/\mathcal{A})/E. \tag{3-18}$$

When *h* tends to zero, the fracture energy tends to a non-null value given as:

$$G_f = \frac{f_t^2}{\mathcal{A}E} \tag{3-19}$$

from which one can define the softening parameter in terms of the material properties as:

$$\mathcal{A} = \frac{f_t^2}{G_f E} \tag{3-20}$$

Figure 3.3 illustrates the typical curve tension versus displacement jump (opening) normal to the interface element, which is subjected to a uniaxial tension. Note that this discrete response corresponds to a rigid-damage behavior.

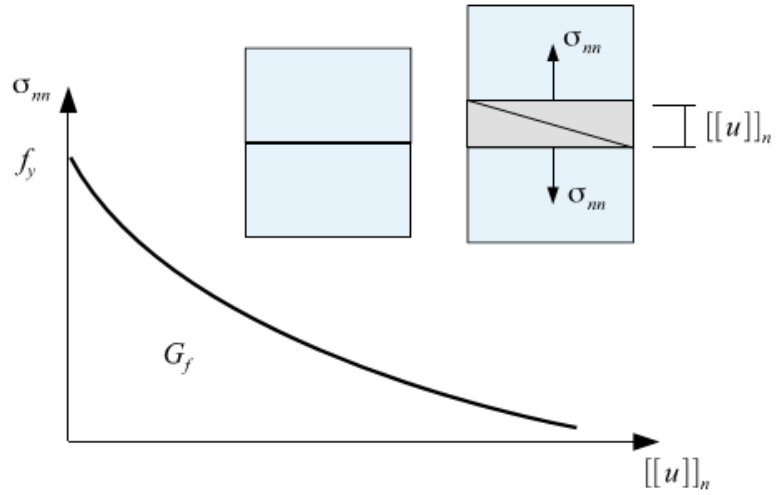

Figure 3.3. Resulting discrete relation of the tension damage model

3.2 Modeling Procedure

A geometric 3D finite element model of a premolar tooth was built. The model also includes a representation of the mandible bone, which was based on tomography images. Six different materials were considered: enamel, dentin, periodontal ligament, trabecular bone, cortical bone and resin. Enamel and dentin are the basic tissues that constitute a sound human tooth. Resin is the restorative materials. The periodontal ligament, which makes the link of the tooth with the mandible bone, is also considered in the modeling process. Figure 3.4 illustrates the distribution of these materials in the geometric domain. In addition, Figure 3.5 andFigure **3.6** are shown the enamel, dentin and restoration representation in a closer view.

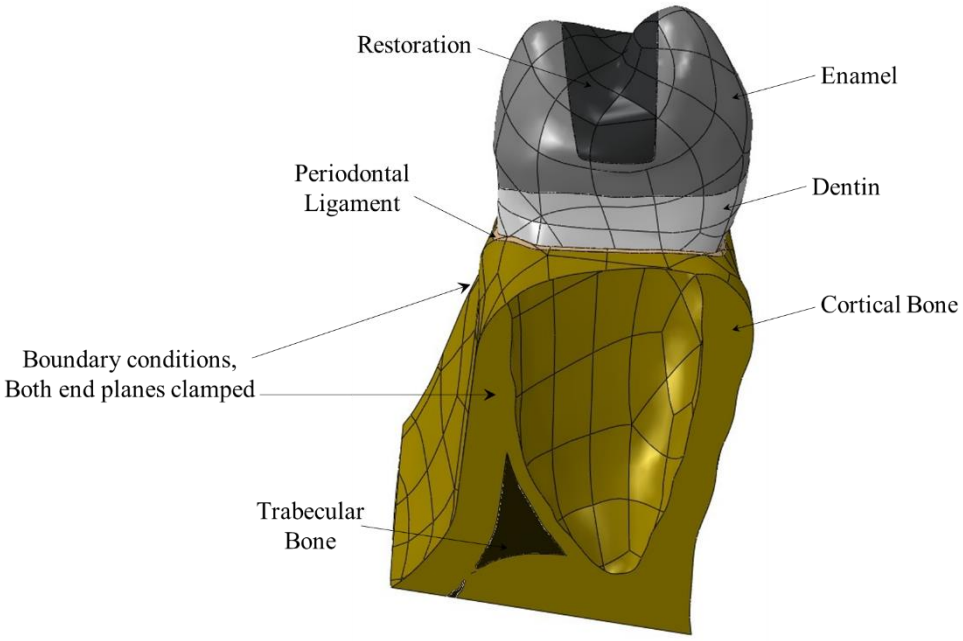

Figure 3.4. Representation of the different parts used in the tooth geometric model

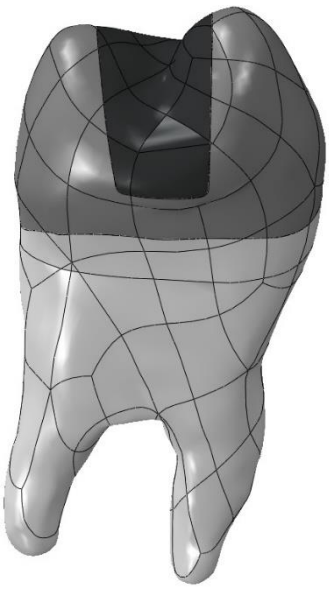

Figure 3.5. Schematic of the dentin, enamel and restoration

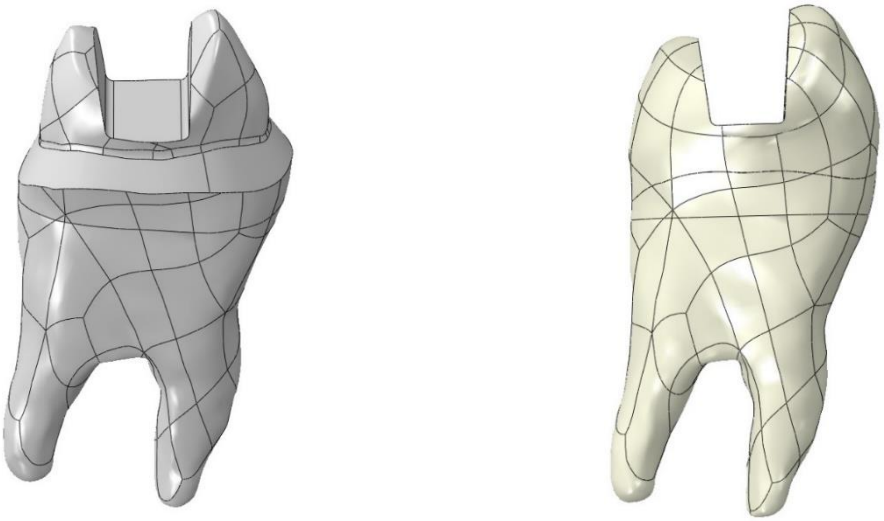

Figure 3.6. Geometry of the dentin only (left) and enamel and dentin (right) without restoration

The shape of the restoration is in accordance with the practical samples, i.e., a real specimen, and similar to the one used in the work of Hamouda and Shehata (2011), Figure 3.7.

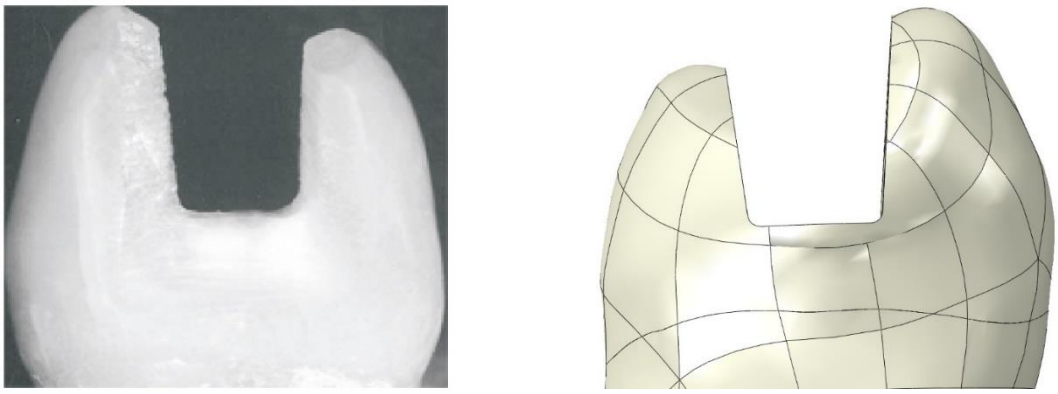

(a) real geometry (Hamouda and Shehata, 2011) (b) model geometry used in this study

Figure 3.7. Schematic of the restoration area

The considered load was 180 N, according to (Cornacchia et al, 2010), divided in twelve point loads, as shown in Figure 3.8. This load is only used to establish preliminary results for both 2D and 3D models. Also, the lateral external surfaces of the mandible bone were fixed in all directions (representing clamped boundary conditions), as illustrated in Figure 3.4.

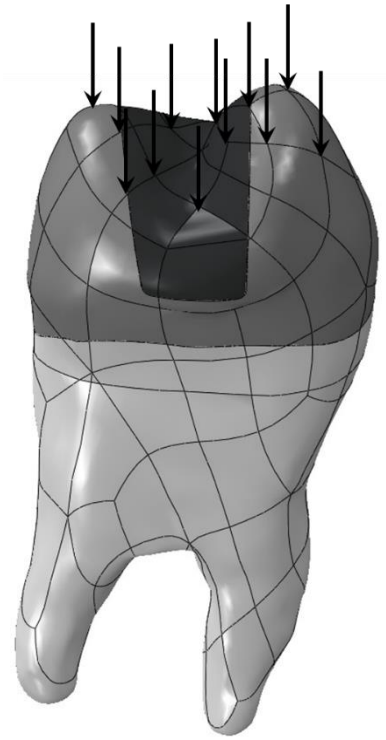

Figure 3.8. Possible loading configuration as concentrated loads with different orientations.

The mechanical properties of each material and tooth tissue are given in Table 3.1. The values for the listed properties were taken from the literature, and the source chosen as reference directly affects the obtained results, as there are no unique values given for the tissues.

Table 3.1. Mechanical properties of each tooth parts

Material	Young's modulus (GPa)	Poisson's ratio	Tensile strength (MPa)	Fracture Energy (J/m^2)
Enamel (Litonjua et al, 2004; Komatsu, 2010)	84.1	0.33	10-24	---
Dentin (El Mowafy et al, 1986; Kinney et al, 1999; Kahler et al, 2003; Litonjua et al, 2004; Miguez et al, 2004; Mattos et al, 2012)	18.45	0.29	32-103	554-742
Composite Resin (Miguez et al, 2004; Chung et al, 2004; Thomaidis et al, 2013; Filtek website, 2014)	25.0	0.30	87	83
Periodontal Ligament (Misch et al, 1999; Pietrzak et al, 2002)	0.000031	0.45	3.0	---
Trabecular Bone (Van Staden et al, 2006; Baker et al, 2010)	0.0962	0.30	140	---
Cortical Bone (Reilly et al, 1974; Baker et al, 2010)	11.17	0.45	7.0	---
Composite resin/Dentin interface (Phrukkanon et al, 1999; Lin et al, 2000; Ferrari et al, 2010)	4.4	0.24	18-23	54.62

3.3 Initial Analyses

This section describes an initial elastic analysis for two- and three-dimensional models using the ABAQUS. The reason to perform the 3D analysis and then 2D analysis is that the tooth model was first built in 3D, so it was decided to perform the initial 3D analysis first. After that, the 2D model was created from the 3D model and thorough study were made on the 2D model.

3.3.1 3D Model

C3D4 element type (4-node tetrahedral element with 12 degrees of freedom) is used for all the domain. Figure 3.9 shows the discretization model.

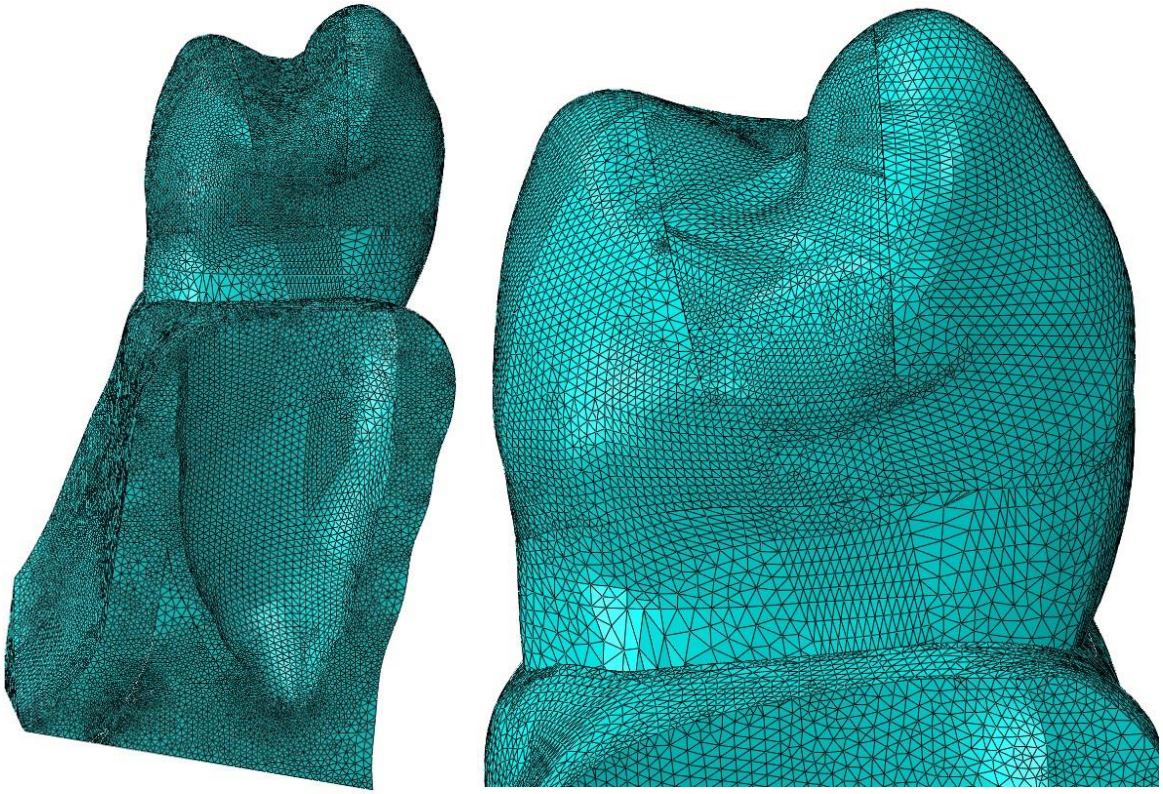

Figure 3.9. Schematic of the meshed model

Figure 3.10 shows the displacement distribution for premolar tooth in millimeters. The maximum value occurs at the top of enamel, which was expected, and is around 0.028 mm.

Von-Mises and first principal stress distributions are shown in Figure 3.11 and Figure 3.12, respectively.

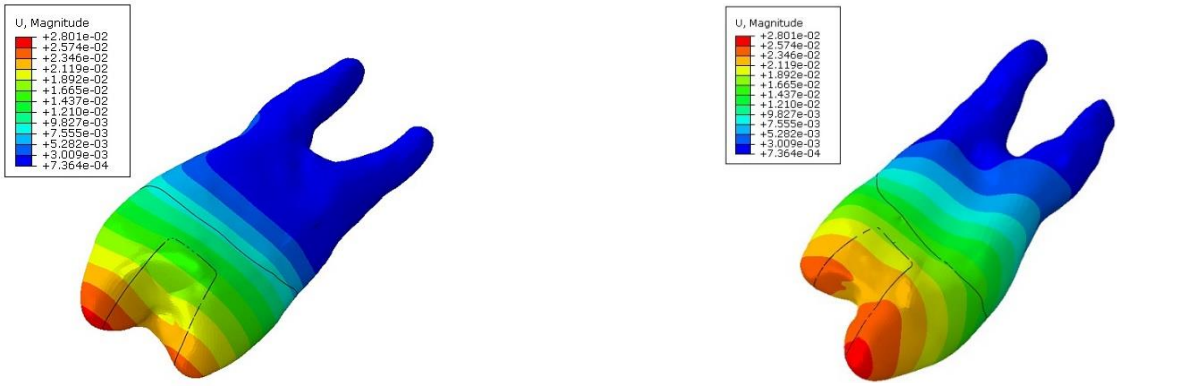

(a) enamel and dentin with restoration, mesial view. (b) enamel and dentin with restoration, distal view.

Figure 3.10. Displacement distribution, in millimeter.

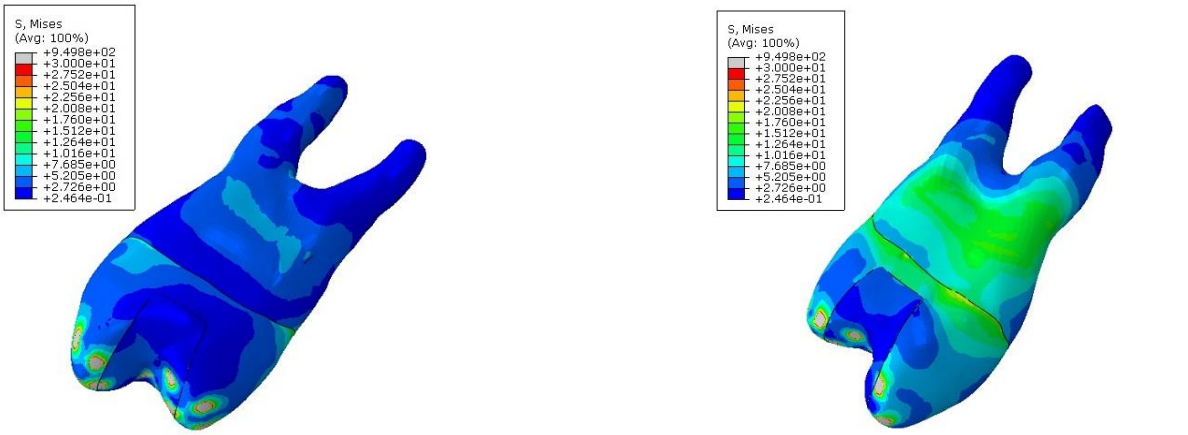

(a) enamel and dentin with restoration, mesial view. (b) enamel and dentin with restoration, distal view.

Figure 3.11. Von-Mises stress component distribution (in MPa)

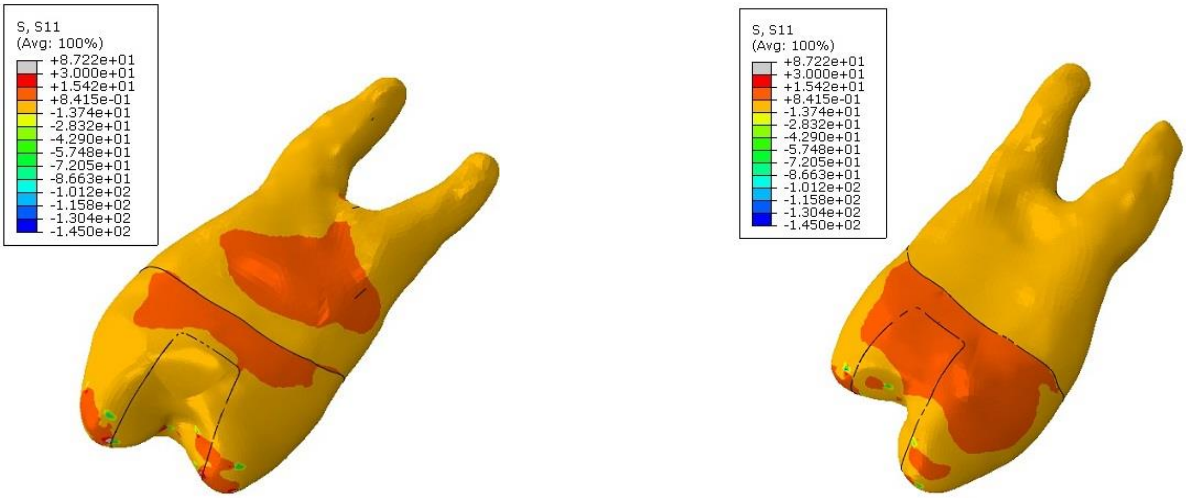

(a) enamel and dentin with restoration, mesial view. (b) enamel and dentin with restoration, distal view.

Figure 3.12. First principal stress component distribution (in MPa)

3.3.2 2D Model

A two-dimensional plane stress (with an out of plane thickness of 5 mm) model is created from a section plane along the middle of 3D model. Here, an initial elastic analysis, similar to the 3D model, is made with the same material, boundary condition, and loading assumptions. Figure 3.13 shows

boundary conditions, loading, and mesh schematic for the 2D analysis. Stress and displacement distributions for this model are shown in Figure 3.14. As it can be seen from this figure, there are some inconsistencies between 3D and 2D results, such as maximum values for both displacement and stress. Those inconsistencies come from some out-of-plane loadings in 3D, because that model is not symmetric along all axes (the symmetrical refers to the shape of tooth geometry, which is not symmetric along all axes). Therefore, this anti-symmetric geometry can produce bending over one or two axes when a similar loading is applied in the 3D model. Finally, it can be said that the 2D model is not a reliable simplification for the actual problem, but it can be used to obtain preliminary results in a simple model.

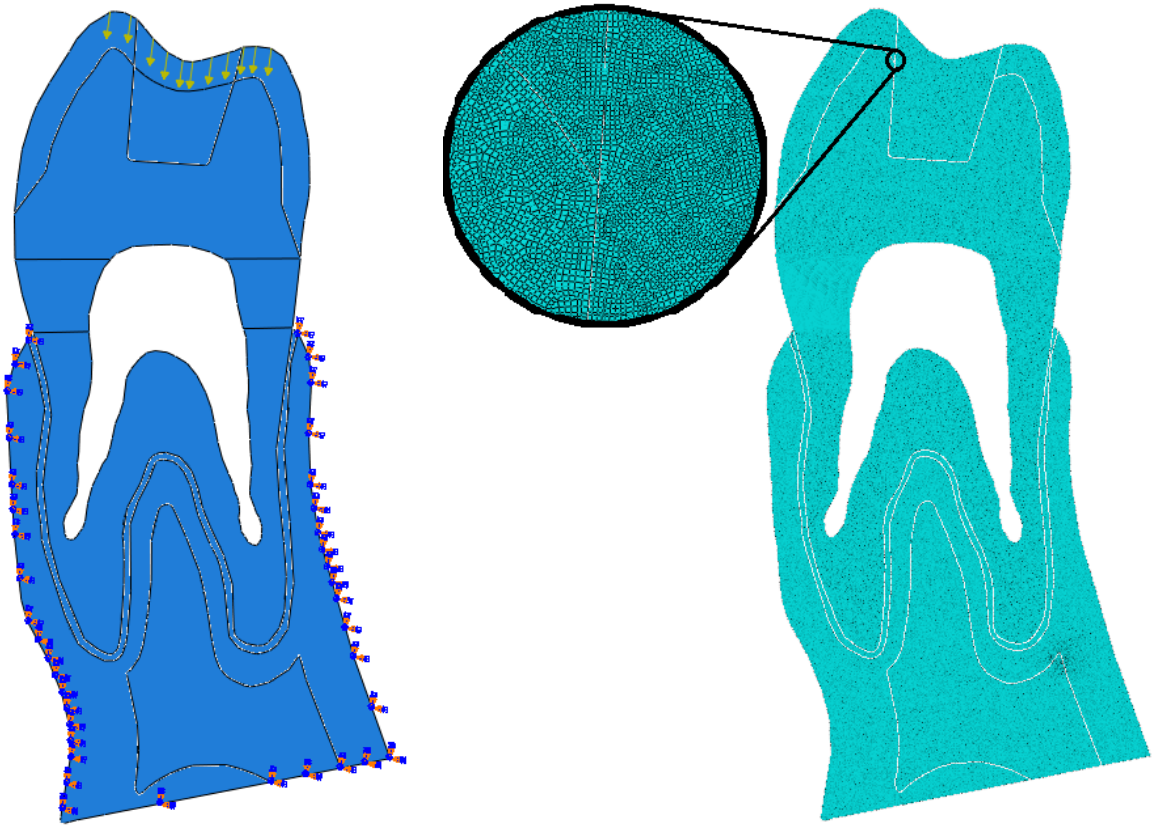

Figure 3.13. Schematic of the boundary conditions, loading, and meshing model

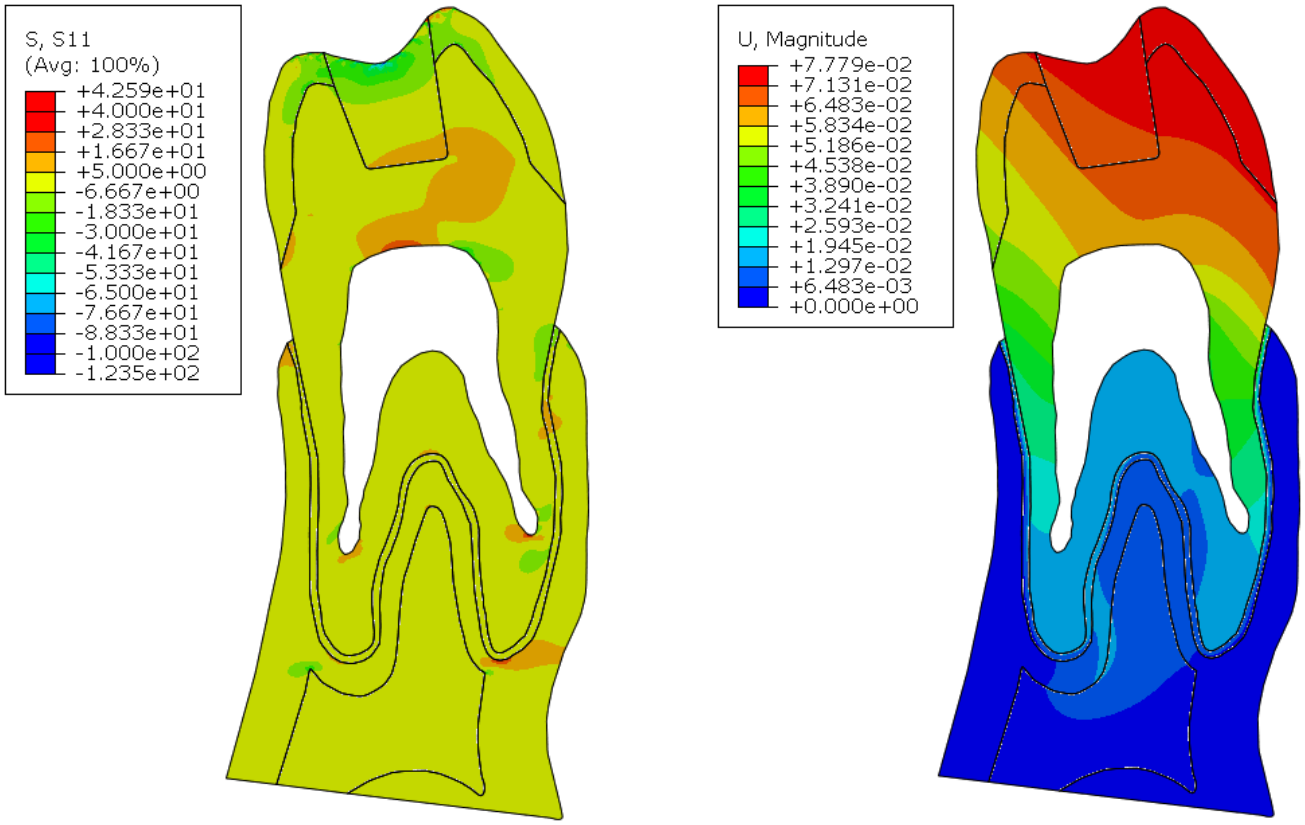

(a) S11 stress (in MPa) (b) Displacement (in mm)

Figure 3.14. First principal stress component and displacement distributions for 2D model in elastic analysis

A mesh sensitivity analysis was made for the 2D results presented here, for element sizes of 0.1 mm, 0.05 mm, and 0.025 mm. The maximum stress S11 for element sizes of 0.1 mm, 0.05 mm, and 0.025 mm were 30 MPa, 42.6 MPa, and 45.3 MPa, respectively. While, the maximum displacements for element sizes of 0.1 mm, 0.05 mm, and 0.025 mm were 0.0774 mm, 0.0778 mm, and 0.0779, respectively. As the displacement for these three element sizes were very close, stresses were considered for mesh sensitivity evaluation. A quick look at the maximum stress values shows that from element size of 0.05 mm to element size of 0.025 mm, there is only 6% difference. Therefore, the element size of 0.05 mm can be represented a good mesh discretization and can deliver suitable results. The results shown in Figure 3.14 were for element size of 0.05 mm.

CHAPTER 4 – METHODOLOGY

This chapter describes the used methodologies for analyzing the crack propagation in a tooth using the mesh fragmentation technique. After providing the model geometry, the process starts by defining the material properties, loading conditions, boundary condition, and finally discretizing the geometry. A meshing software, the GiD pre- and post-processor software (GiD software, 2016), is used to discretize the model. After having the discretized model, the input file for Matlab code must be prepared, which includes the whole interface element and fragmentation formulation. The Matlab code refers to the whole implementation regarding to the mesh fragmentation technique, developed and implemented by Manzoli et al. (2012, 2016). This input file must be saved in '*mfl'* format and it has different parts in which all of them will be described here. The first part is the `CONTROL_DATA`, which is shown in Figure 4.1.

```
CONTROL_DATA
   GEOMETRY:      2
   DIMENSIONS:    NPOIN=12 NELEM=12 NELFR=0 NDPEL=3 NGAUS=1 NSETS=1
END_CONTROL_DATA
```

Figure 4.1. `CONROL_DATA` input data.

As seen in Figure 4.1, the tag `GEOMETRY` is responsible to define the model dimension and its type, 1 and 2 refer to 2D problems with plane strain and plane stress states, and 3 refers to the 3D model. Under the `DIMENSIONS` section, the `NPOIN`, `NELEM`, `NDPEL`, `NGAUS`, and `NSETS` refer to number of nodes, number of elements, number of nodes per element, number of Gauss points within each element, and number of materials inside the geometry.

Then, geometry data including the elemental, nodal, and material properties are defined under the `GENERAL_DATA` section, as shown in Figure 4.2. This data includes the element labels, their connectivities and corresponding material sets, as well as nodal label and coordinates, and material properties for each material set. In the material set definition, beside elastic modulus and Poisson's ratio, there are `TYPE`, `MODEL`, `THICKNESS`, and `NGAUS` where they refer to element type (2 for triangular and 3 for tetrahedral), model type (1 for elastic model, 15 for model with interface elements only in tension mode, and 21 for model with interface elements in both tension and shear modes), model thickness, and number of Gauss points within each element, respectively. In the case of model type 15, there are two other parameters needed, `FTULT`, which is tensile strength, and `HBAT`, which is

the softening parameter defined by Eq. (3-20). In addition, for model type 21 there are more two additional parameters: FCULT, shear strength, and HBAC, the softening parameter in shear direction.

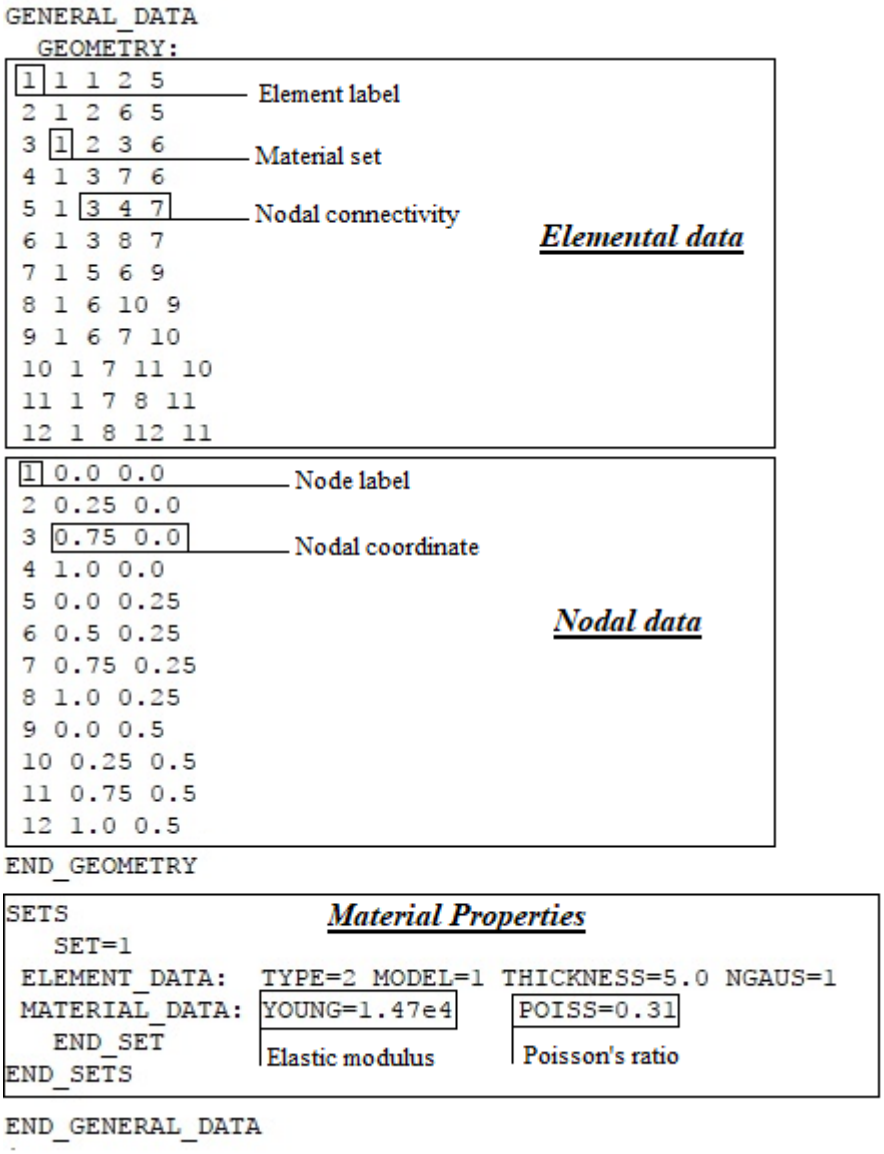

Figure 4.2. GENERAL_DATA input data.

Then, the INTERVAL_DATA section defines the number of steps to be solved (NSTEP) as well as the incremental time of each step (DTIME). Figure 4.3 shows the input line for load and boundary condition definitions. The load can be either POINT_LOAD or FACE_LOAD. In the case of POINT_LOAD, a node label must be defined along with values of point load in different directions. The BOUNDARY section defines the boundary condition, containing all nodes with their boundary values, as described in Figure 4.3.

```
LOAD: NEW_LOAD
   POINT_LOAD
     NODE=1        FX=10.0       FY=10.0
   END_POINT_LOAD

   FACE_LOAD

   END_FACE_LOAD
END LOAD

BOUNDARY: NEW_BOUNDARY
      1 11  0.00 0.00
      2 11  0.00 0.00
      3 11  0.00 0.00
END BOUNDARY
```

Node label

Prescribed diplac. in both x & y directions

Zero displacement in both x & y direction, i.e., clamped BC for this case

Figure 4.3. `LOAD` and `BOUNDARY` input data.

Figure 4.4 presents the required data for the analysis procedure, under the section `STRATEGY`. It includes two tolerance parameter (`TOL_NEWTON` which is the Newton tolerance and `TOL_CONST_MODEL`, the constitutive model tolerance), `STRATEGY` (1 for load control and 4 for displacement control), `DS` which is incremental displacement to be used for controlling procedure, `NODE1` which is node to be used for displacement control approach, and `DOF1` which is the direction for displacement control approach.

```
STRATEGY: NEW_STRATEGY
   LINE_SEARCH: OFF
   CONVERGENCE: TOL_NEWTON=1E-6 TOL_CONST_MODEL=1E-8 ETA_MIN=1 ETA_MAX=1 /
                ETA_PAR=1 TOLER=1 STRATEGY=4 DS=5.0e-05 NODE1=6 DOF1=2
   POST_PROCESS: STEP=1
END_STRATEGY
```

Figure 4.4. `STRATEGY` input data.

After the input file preparation, it can be used to run an elastic analysis or insert the interface element in between the elements, inside the region of interest, and perform the fracture analysis. Figure 4.5 shows the steps to be done for the fracture modeling, from the model creation to the analysis using the Matlab code. The 3D model came from a QCT (quantitative computed tomography)-scan procedure to have both real geometry and material properties of a tooth. It was imported into the Solidworks to create either 3D or 2D igs (Initial Exchange Specification) format files for the analysis. Next, it was imported into the GiD, which was used for mesh generation and results visualizations. After applying the material properties, boundary conditions, loading, and discretizing the model, an initial input file can be extracted from the GiD, which has be modified to be usable by Matlab code that is responsible to perform the fragmentation process. After that preparing the whole input file, a mesh fragmentation code, written in Fortran, was used to insert the interface element in between the

conventional elements in the region of interest. At the end, the Matlab code is used for the analysis based on mesh fragmentation technique.

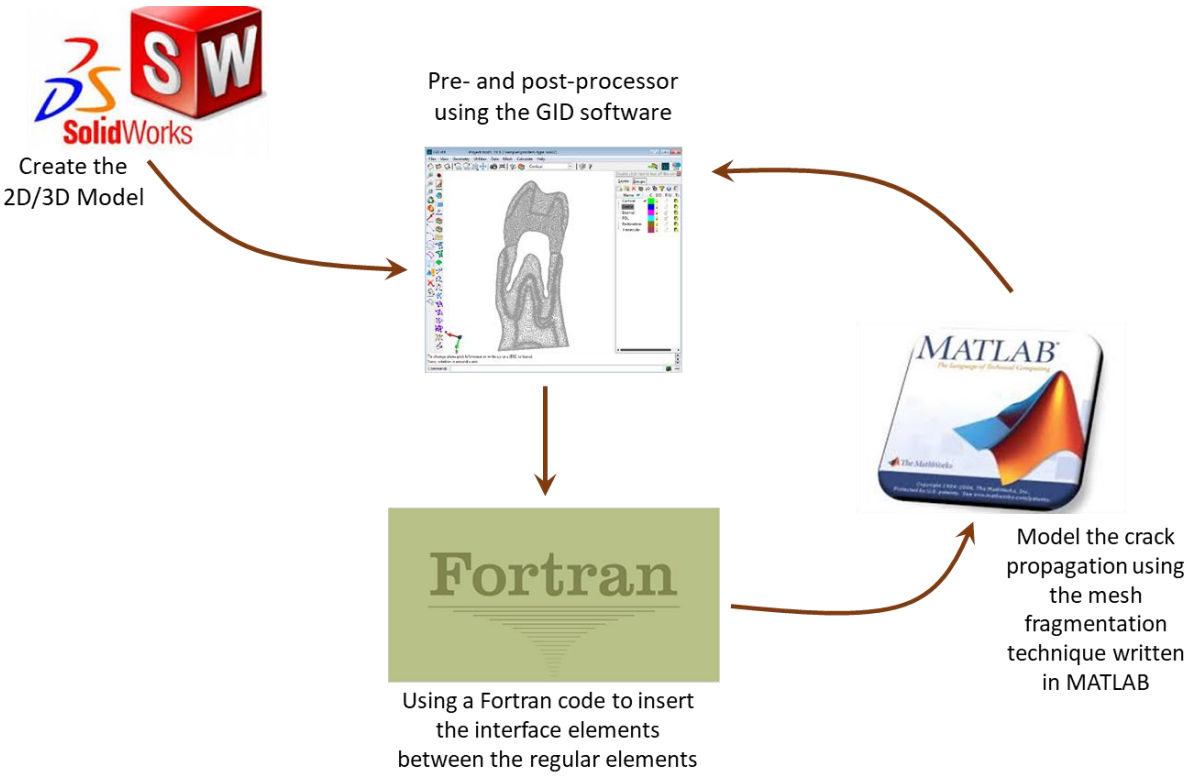

Figure 4.5. Fracture analysis procedure using the mesh fragmentation technique.

CHAPTER 5 - FRACTURE ANALYSIS USING MESH FRAGMENTATION TECHNIQUE

5.1 Analyzing the 2D model

The 2D model is created from a section plane along the middle part of the 3D model. Figure 5.1 shows the geometry, boundary conditions, loading, and mesh schematic for the 2D analysis. There are 13,903 triangular elements (linear 3-node triangular elements) in the discretized model, with 5,419 elements for dentin; 774 elements for restoration; 1,017 elements for enamel; 1,261 elements for periodontal ligament; 3,778 elements for cortical bone; and 1,654 elements for trabecular elements. In this section, we describe the results for two different analyses: (1) an elastic analysis, and (2) a fracture analysis, with different loading configurations (lingual, buccal, and lingual+buccal loadings cases shown in Figure 5.1(a)). As we explained in chapter 1 and according to the literature, the loading magnitude was set up to a maximum of 600 N.

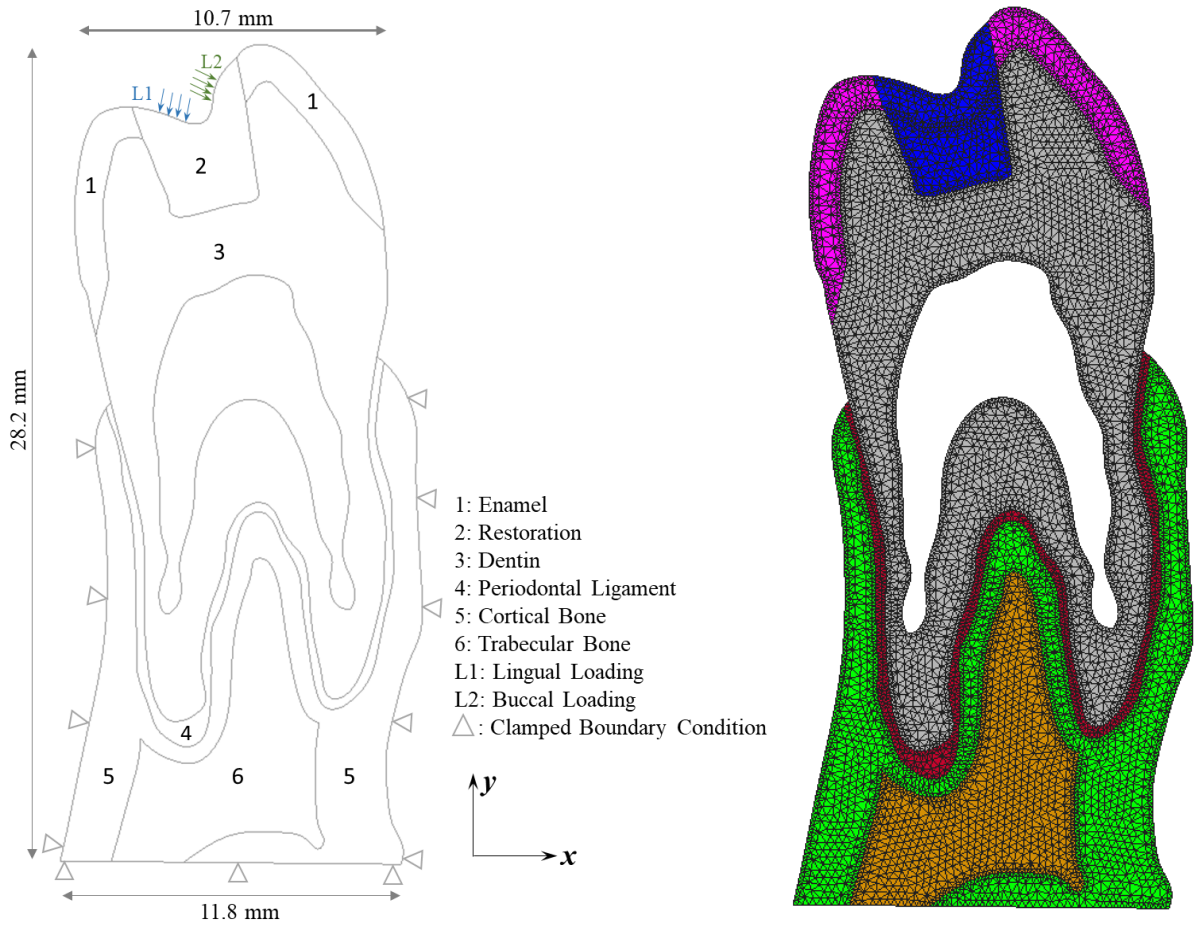

(a) geometry and loading (b) mesh discretization.

Figure 5.1. Schematic of the boundary conditions, loading, and meshing model

5.1.1 Elastic Analysis

The stress and displacement distributions for this model, for the elastic analysis, are shown in Figure 5.2 to Figure **5.4**. The loading orientation has an important impact on both displacement and stress distributions.

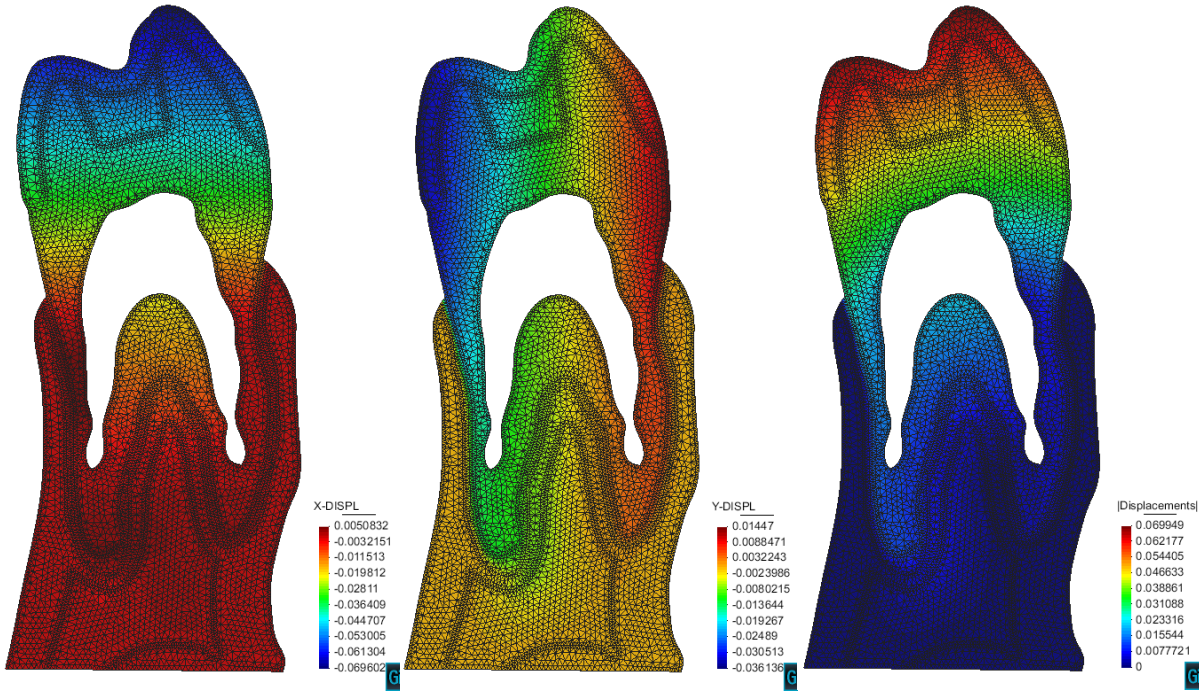

(a) x-direction (b) y-direction (c) total

Figure 5.2. Distribution of displacements for *lingual* loading for 2D model in elastic analysis.

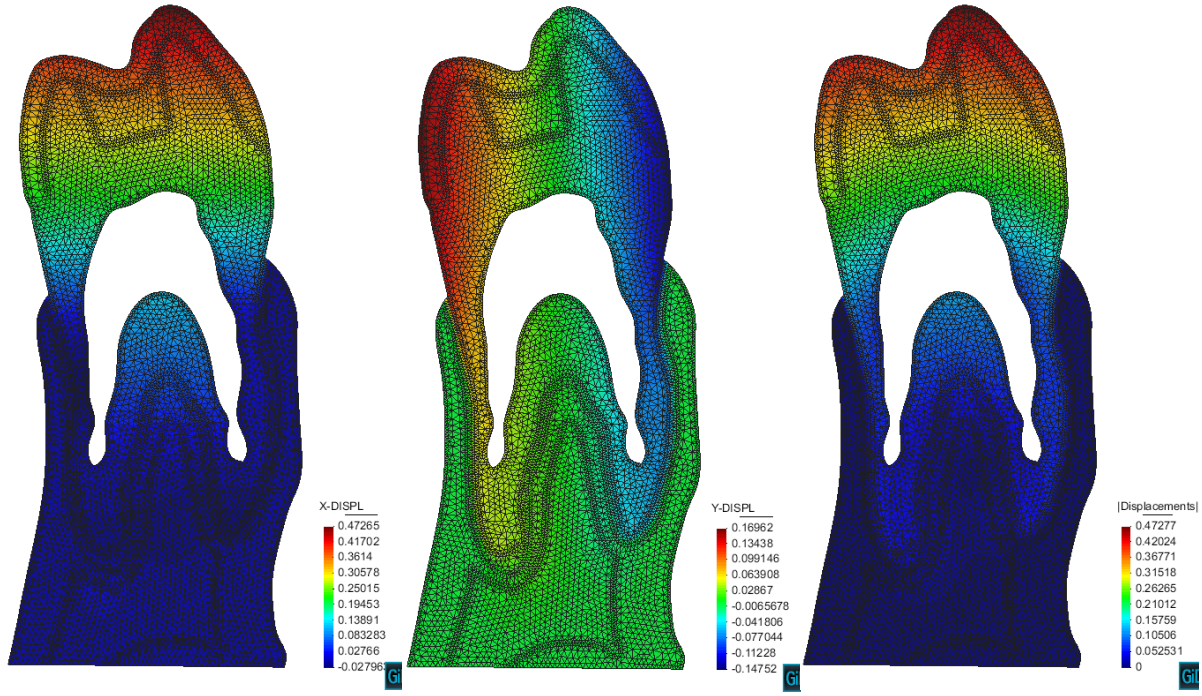

(a) x-direction (b) y-direction (c) total

Figure 5.3. Distribution of displacements for *buccal* loading for 2D model in elastic analysis.

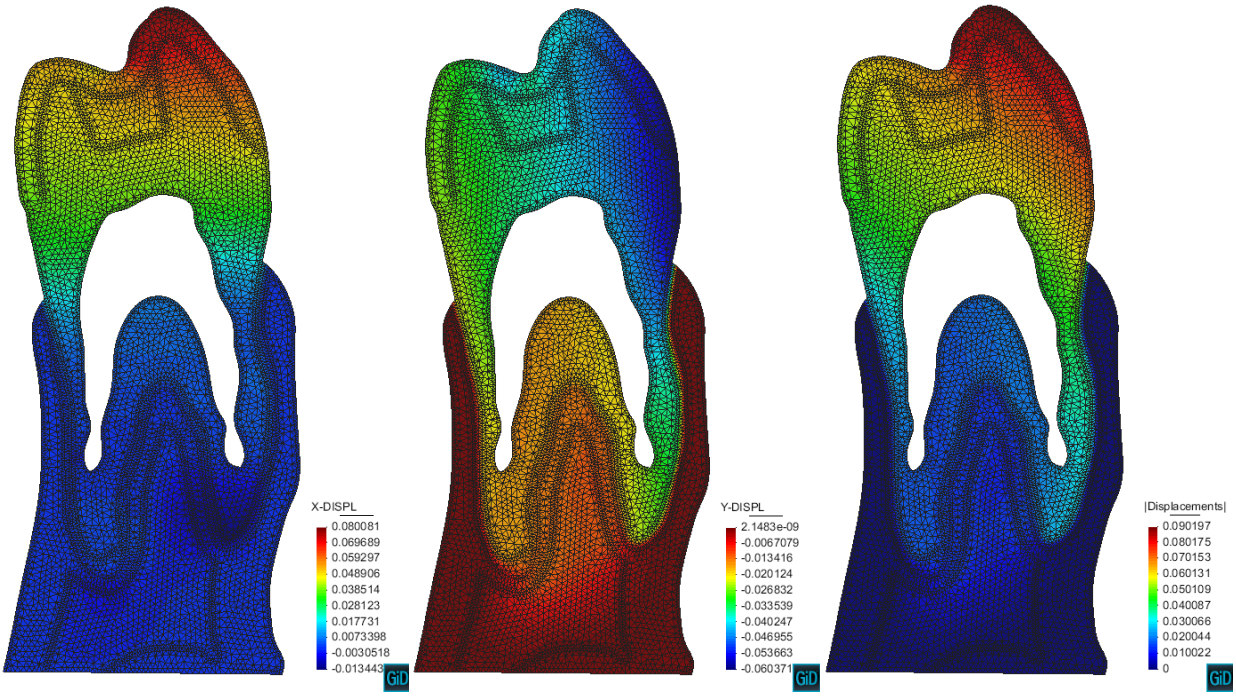

(a) x-direction (b) y-direction (c) total

Figure 5.4. Distribution of displacements for *lingual+buccal* loading for 2D model in elastic analysis.

An important fact is that the displacement distribution clearly shows the effect of various loading cases. In order to study the elastic behavior of the tooth under aforementioned loading cases, the stress distributions are shown in Figure 5.5 to Figure 5.7.

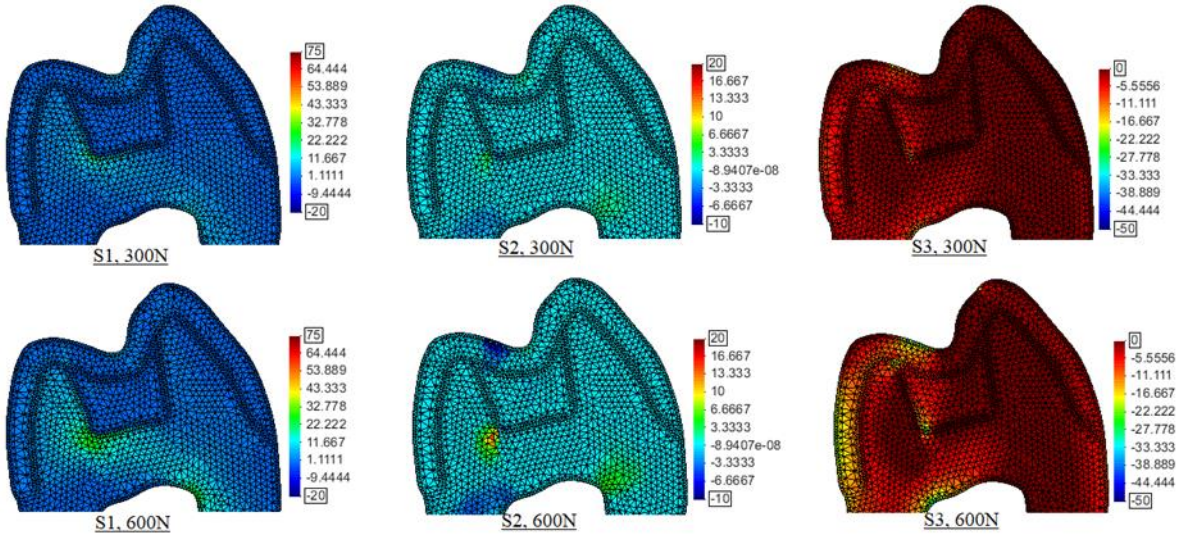

Figure 5.5. Distribution of principal stresses (in MPa) for *lingual* loading for 2D model in elastic analysis.

Figure 5.6 show the stress distributions for the buccal loading case. The stress concentrations are a little far from the bottom side of the restoration, closer to the pulp boundaries. **Error! Reference source not found.** show the principal stress distribution for lingual+buccal loading case.

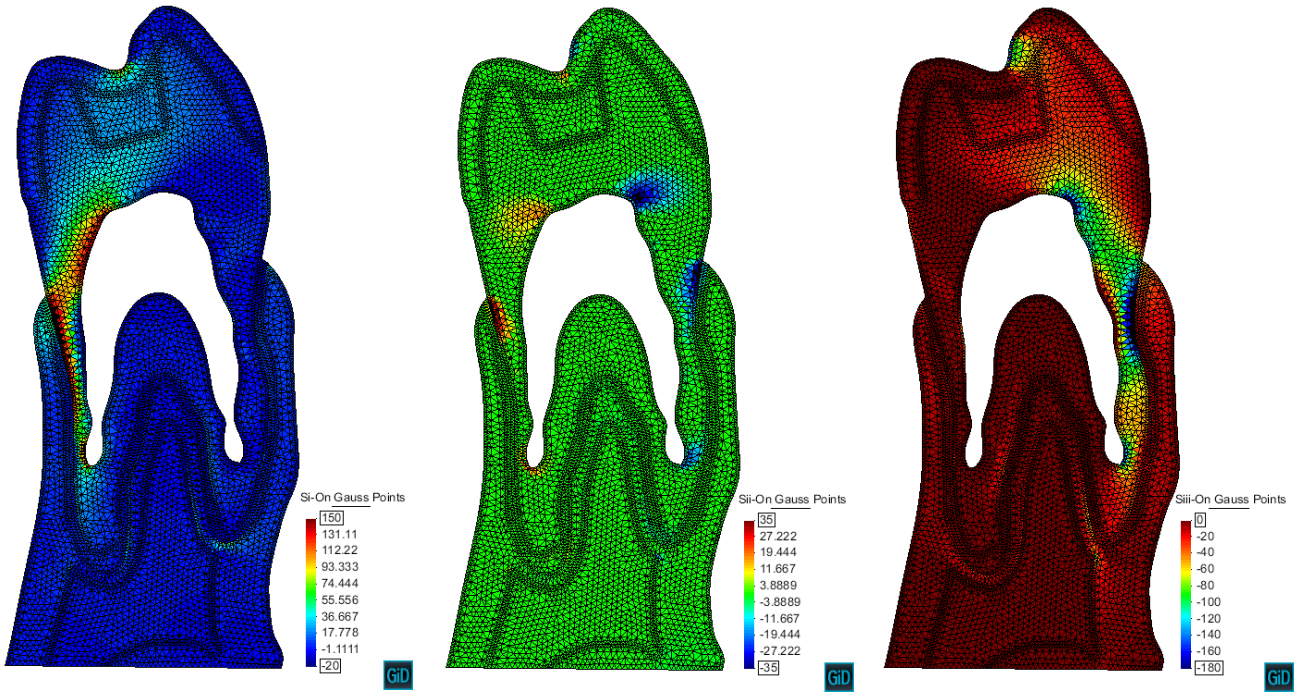

(a) S1 (b) S2 (c) S3

Figure 5.6. Distribution of principal stresses (in MPa) for *buccal* loading for 2D model in elastic analysis.

Figure 5.7 shows the stress distribution for the case of lingual+buccal loading, aiming to clarify the stress distributions near the bottom of the restoration, where a crack initiation might occur. The stresses are mainly concentrated at the loading points, which they are expected. Other than these points, the stress distributions are almost the same for the lower bottom corners of the restoration area.

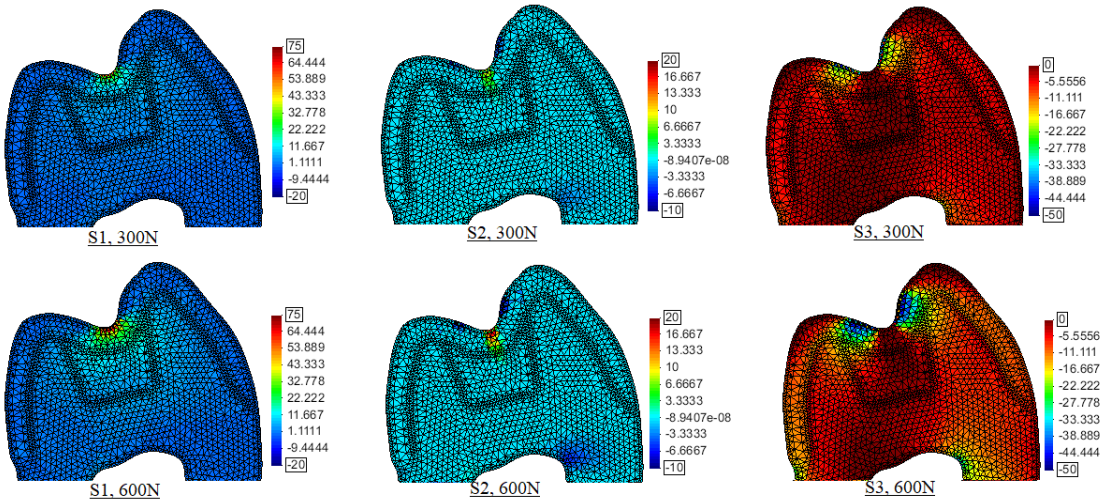

Figure 5.7. Distribution of principal stresses (in MPa) for *lingual+buccal* loading for 2D model in elastic analysis, with a different stress limits.

5.1.2 Fracture Analysis

After the elastic analyses, interface elements are inserted in between the elements of dentin to model the crack propagation in the dentin. These interface elements were inserted also between dentin and restoration boundaries as well as enamel and restoration boundaries in order to model the bonding

failure between these two parts during the crack propagation process. In addition, two different cases were modeled: dentin with and without a pre-existing crack at different positions: lingual, buccal, and central as shown in Figure 5.8 (with a length of 0.3 mm). Similar to the elastic analyses, three different loading cases are also considered here to see the behavior of crack propagation in the dentin.

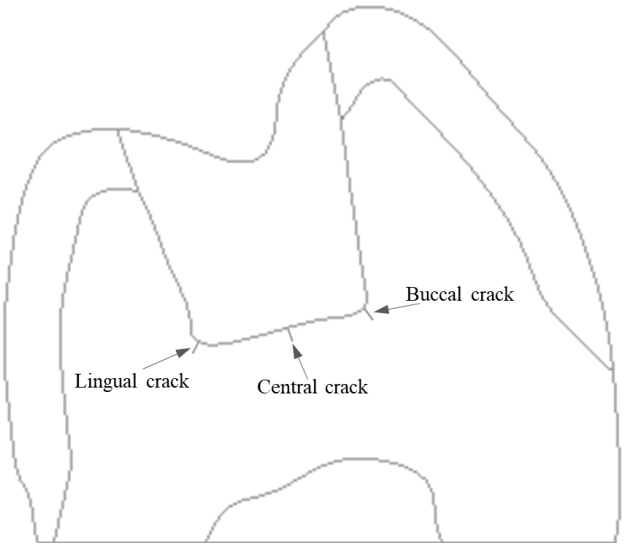

Figure 5.8. Position of the initial crack

As mentioned in chapter 4, besides elastic modulus and Poisson's ratio, there are other parameters that must be defined for those parts that contain interface elements: tensile strength and the softening parameter. The tensile strength (`FTULT`) can be obtained from Table 3.1. The softening parameter (`HBAT`) can be also calculated using Eq. (3-20) along with use of tensile strength, fracture energy and elastic modulus from Table 3.1. Since the interface elements were only inserted in the dentin region, let's consider an average value for both tensile strength and fracture energy from Table 3.1: tensile strength equal to 70 MPa and fracture energy equal to 650 N.m. Then, the `HBAT` would be equal to 408 m^{-1}. Let's first start to model the crack initiation and propagation in the dentin with these parameters with different loading conditions. Figure 5.9 and Figure 5.10 show the frature analysis for the lingual and buccal loading cases with tensile strength of 32-70 MPa and a softening parameter of 85-408 m^{-1} (with an average fracture energy of 648 J/m^2).

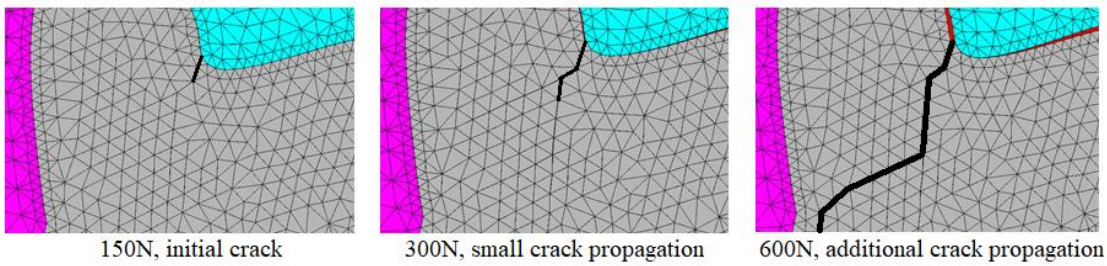

(a) With tensile strength of 32 MPa

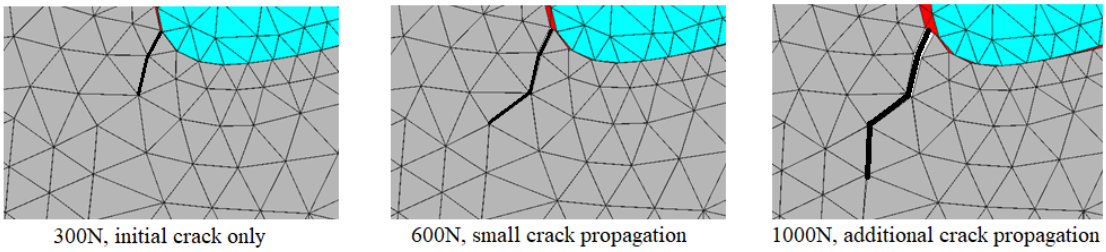

(b) With tensile strength of 50 MPa

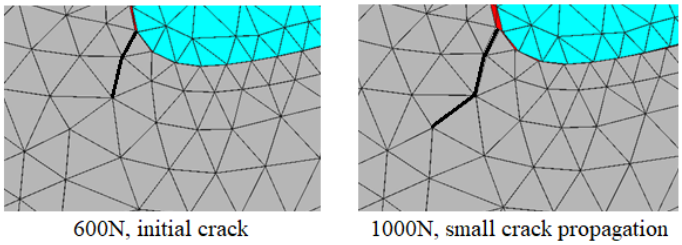

(c) With tensile strength of 70 MPa

Figure 5.9. Fracture results for *lingual* loading case, with different tensile strength values and a softening parameter of 85-408 m^{-1}.

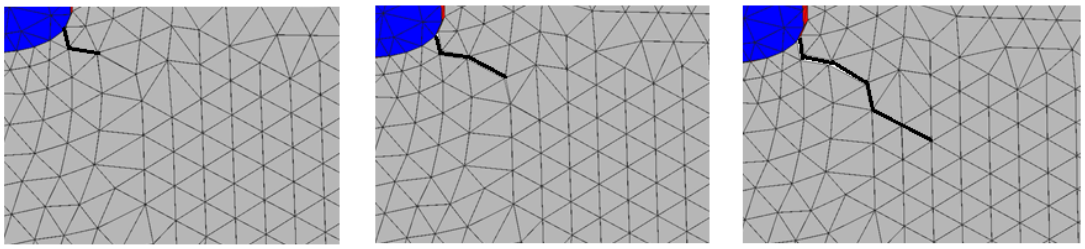

(a) With tensile strength of 32 MPa

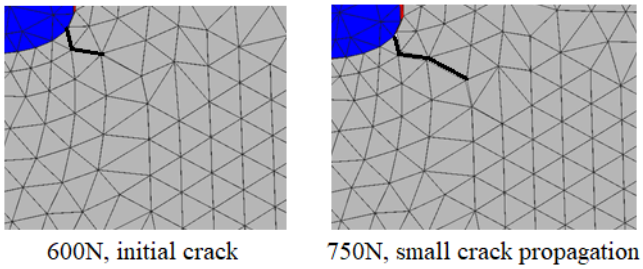

(b) With tensile strength of 50 MPa

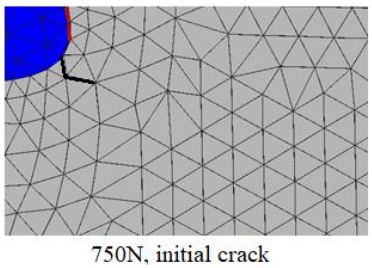

(c) With tensile strength of 70 MPa

Figure 5.10. Fracture simulation for *buccal* loading case, with different tensile strength and softening parameter of 85-408 m^{-1}.

According to Figure 5.9 and Figure 5.10, for the tensile strength value of 70 MPa, which is the average values obtained from Table 3.1, there is no crack propagation for both lingual and buccal loading cases until loading value of 600N, while for buccal case there is small crack propagation under

loading value of 750N. For the tensile strength value of 50 MPa, there is a small crack propagation for lingual loading of 600N, while for buccal loading of 600N there is no crack propagation. Finally, for the tensile strength value of 32 MPa, we can see a quite big crack propagation for lingual loading equal to 600N, but a small amount of crack propagation ocuured for buccal loading with the same loading value. *Therefore, it can be said that under current loading configurations and with an average values for tensile strength and fracture energy, the restored tooth does not experience any major crack propagation. But, a value of 32 MPa is considered as the tensile strength value of the dentin in this research, for the failure point of the interface elements in the dentin part ro conduct a fruther fracture analysis. Although this value is the smallest value from Table 3.1, but it is choosed to study the fracture path under various loading conditions, while the results for the bigger values were also shown in the previous figures.*

Therefore, the fracture path from different loading cases along with various pre-existing crack positions, as well as model without any crack are shown in Figure 5.11 to Figure 5.17. The models without cracks are analyzed in order to verify whether any crack would be initiated under different loading orientations and various loading magnitudes. Then, for each loading cases, a corresponding crack position will be inserted in the model. As an example, for lingual loading the lingual crack is placed in the model. However, for lingual+buccal loading case, all the three pre-existing cracks are placed in the model and their propagation behavior is studied separately.

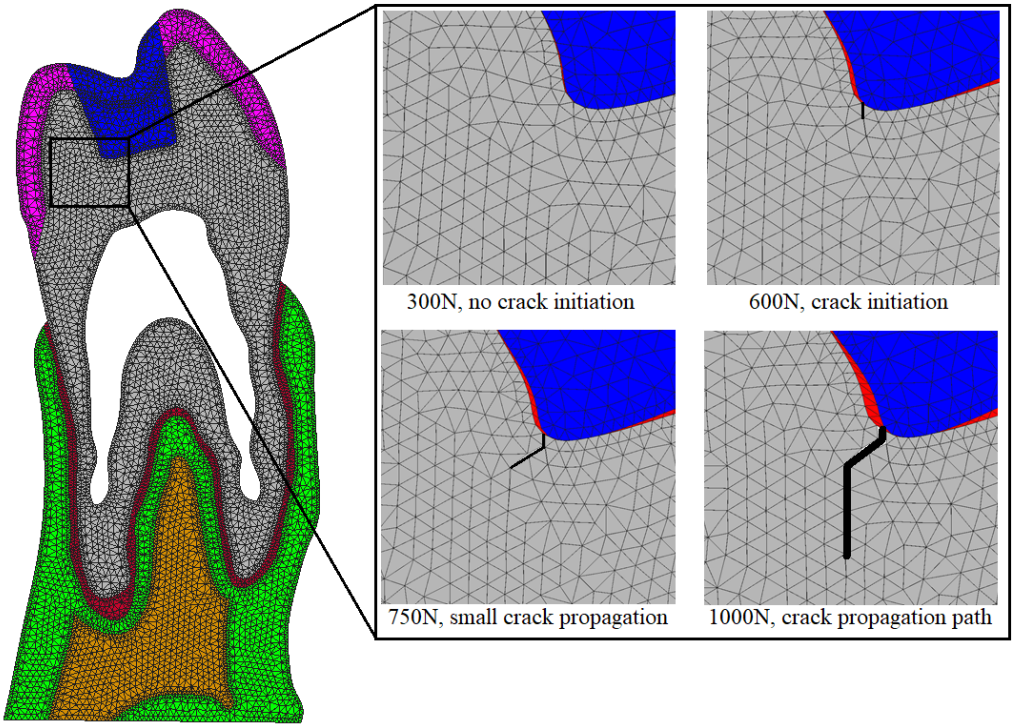

Figure 5.11. Crack propagation path for *lingual* loading case, without any pre-existing crack.

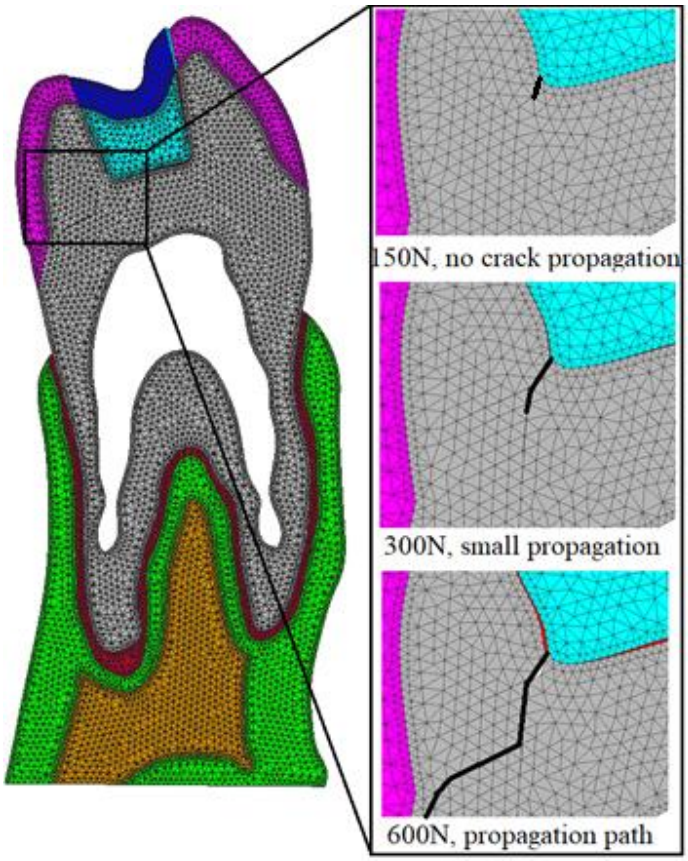

Figure 5.12. Crack propagation path for *lingual* loading case, with a pre-existing crack.

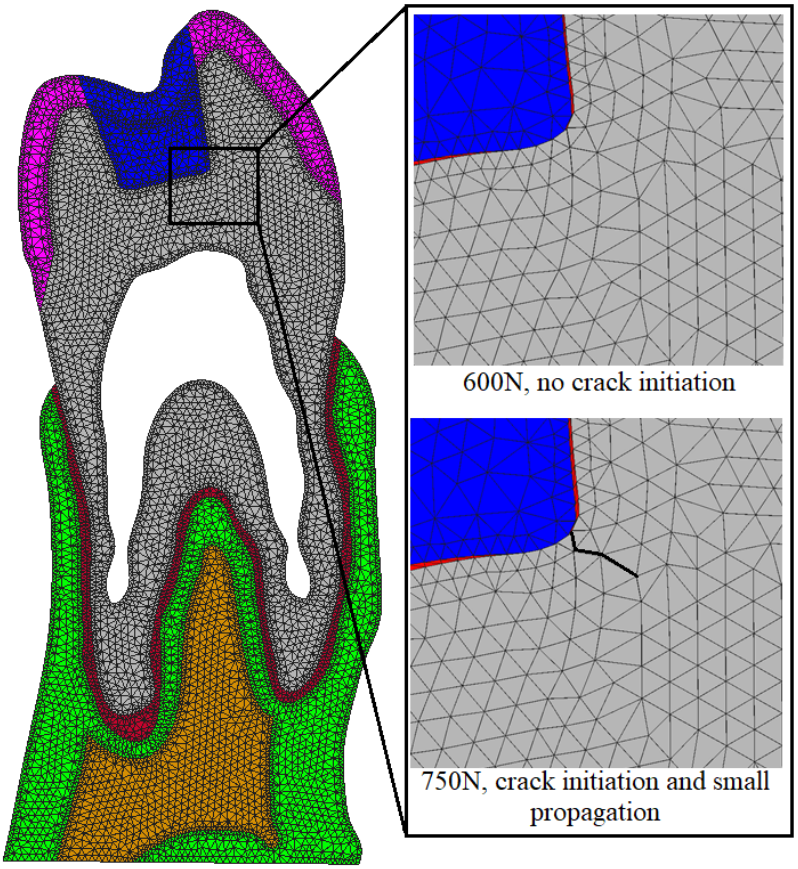

Figure 5.13. Crack propagation path for *buccal* loading case, without any pre-existing crack.

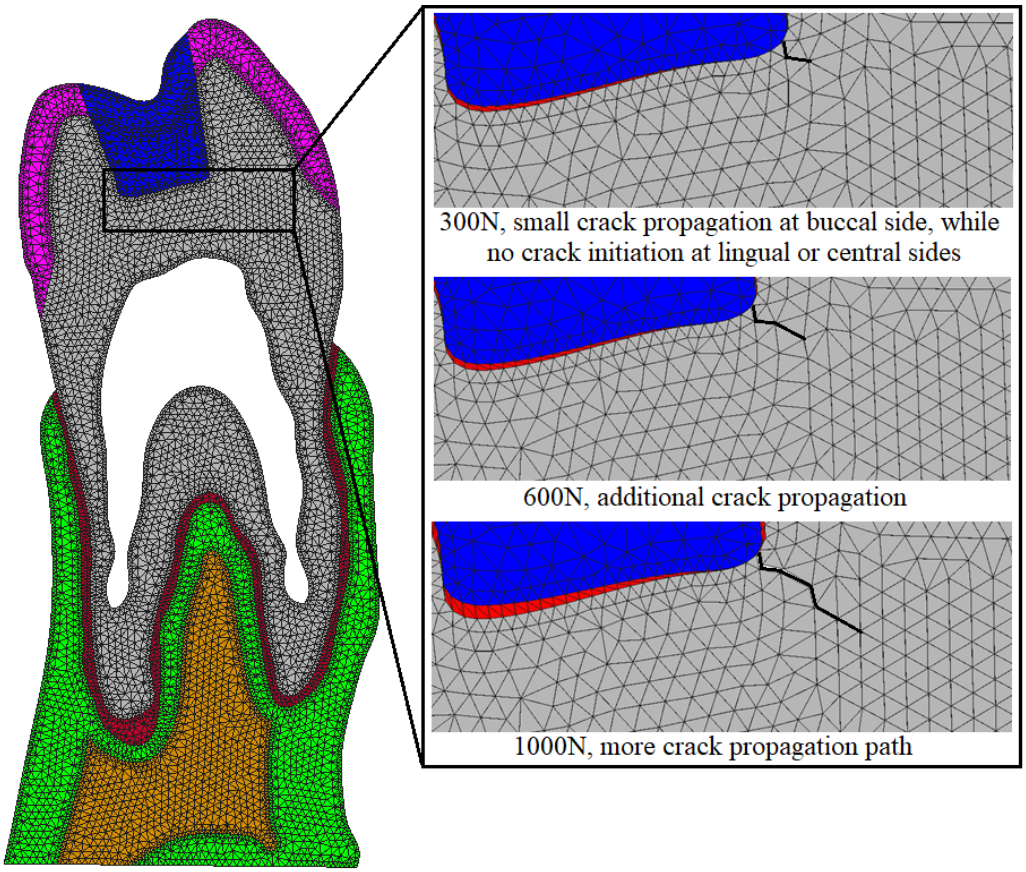

Figure 5.14. Crack propagation path for *buccal* loading case, with a pre-existing crack at buccal side.

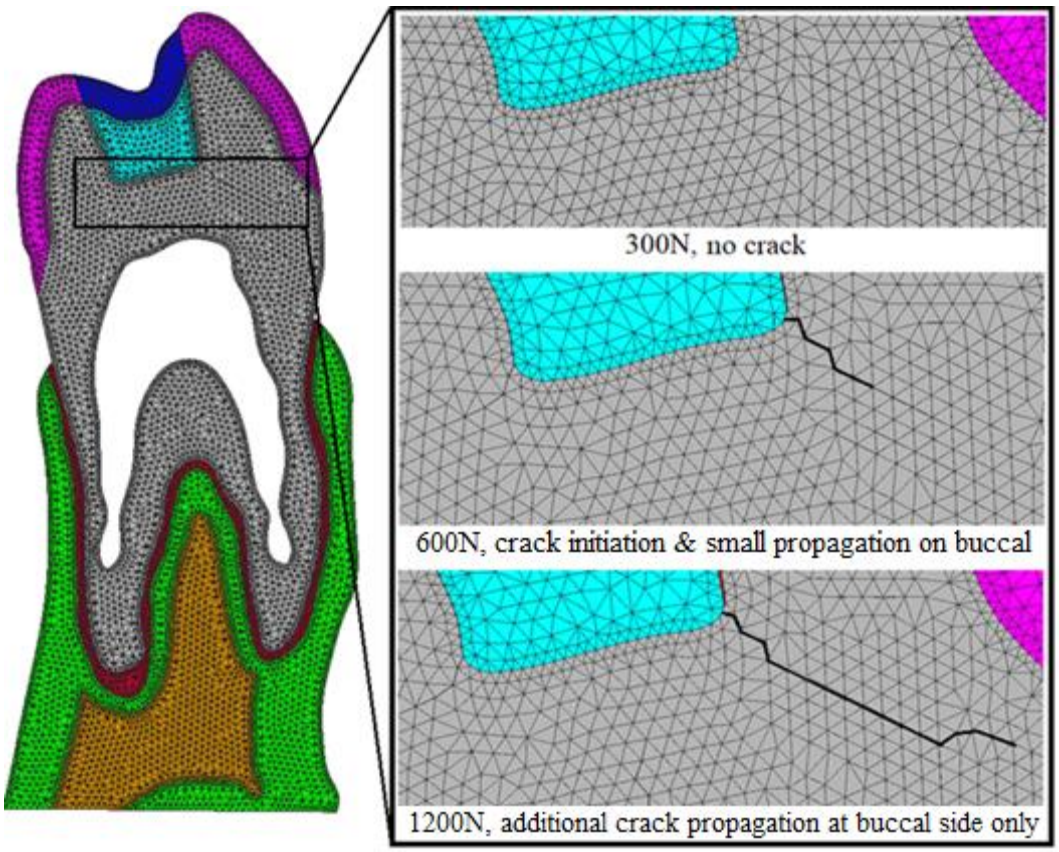

Figure 5.15. Crack propagation path for *lingual+buccal* loading case, for each loading sides, without any pre-existing crack.

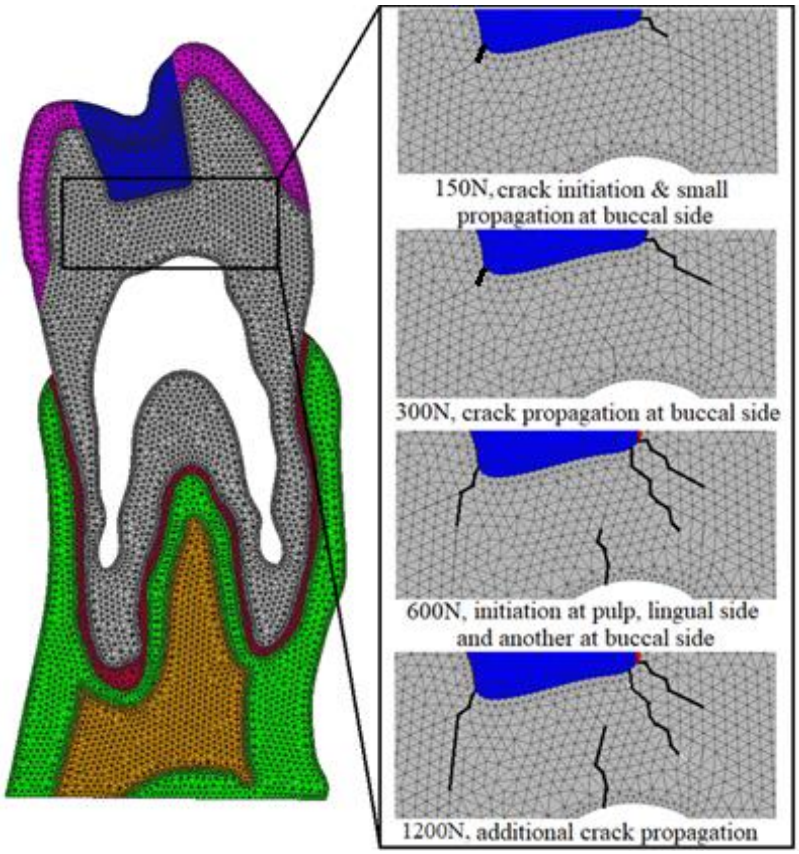

Figure 5.16. Crack propagation path for *lingual+buccal* loading case, for each loading sides, with a pre-existing crack at lingual side.

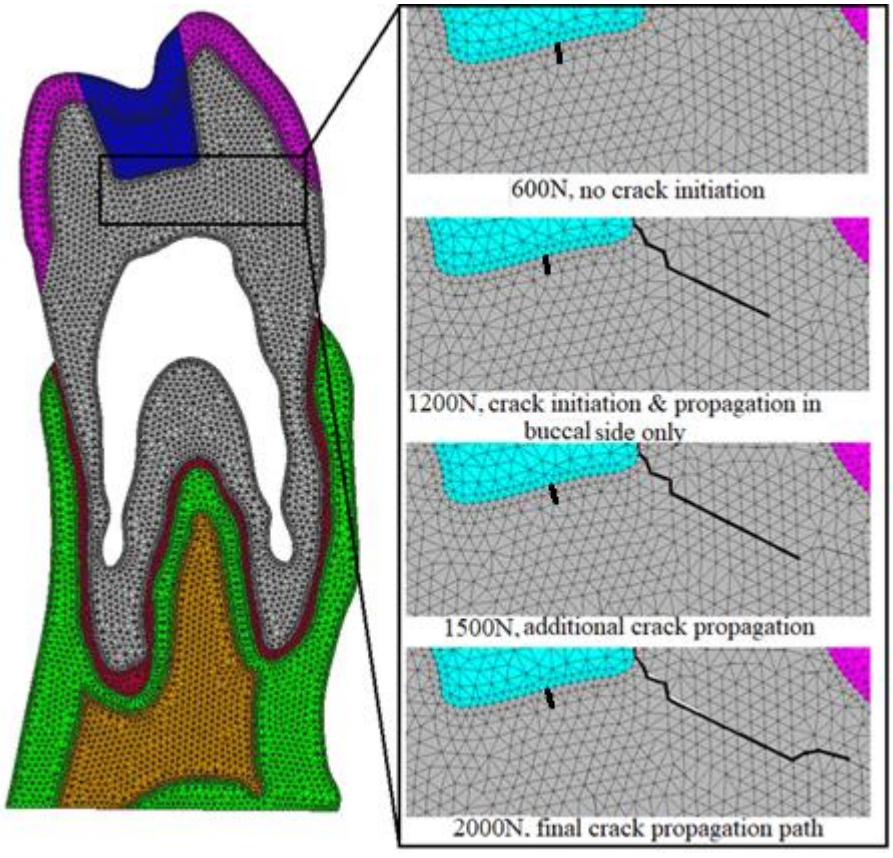

Figure 5.17. Crack propagation path for *lingual+buccal* loading case, for each loading sides, with a pre-existing crack located at the bottom center of the cavity.

As it can be seen from previous figures, the lingual and lingual+buccal loading cases have shown some bigger crack propagation paths, mainly due to their loading configuration as well orientation regarding to the applied load surface, i.e., the restoration surface. The realistic loading value for a tooth was chosen up to a maximum of 600N, from the literature. Therefore, all the crack propagation until the loading of 600N is acceptable and can be considered more close to the realistic situation. However, the bigger load magnitudes were shown as well in order to demonstrate the crack propagation behavior under other less common loading conditions.

5.2 Elastic Analysis of the 3D Model

A preliminary 3D elastic analyses were also made for the whole tooth, using both Abaqus and Matlab written program. The Abaqus results are used to validate the 3D elastic analysis with the Matlab program. Figure 5.18 and Figure 5.20 show the displacement and first principal stress distributions, obtained by Abaqus and Matlab program. As it can be seen from these two figures, the preliminary elastic results from Matlab program are very close to those one obtained by Abaqus. Therefore, this 3D model can be used to conduct further elastic 3D analysis and 3D fracture analysis as well.

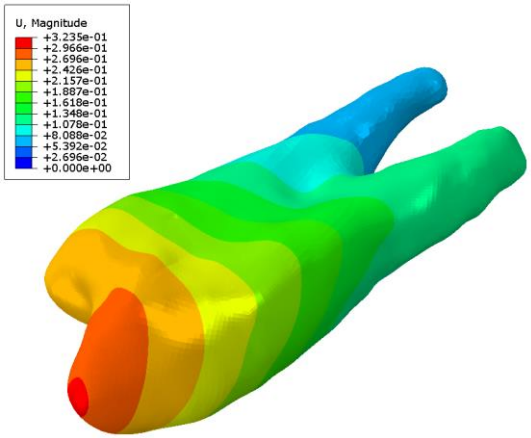

(a) Abaqus model, mesial view.

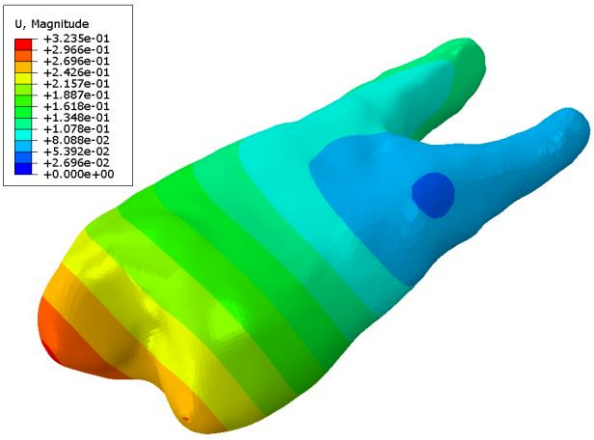

(b) Abaqus model, distal view.

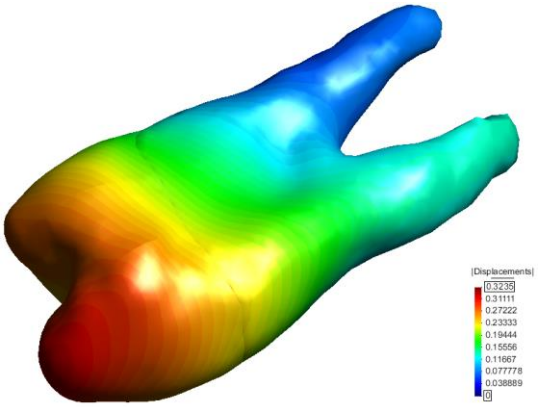

(c) GiD model solved in Matlab code, mesial view.

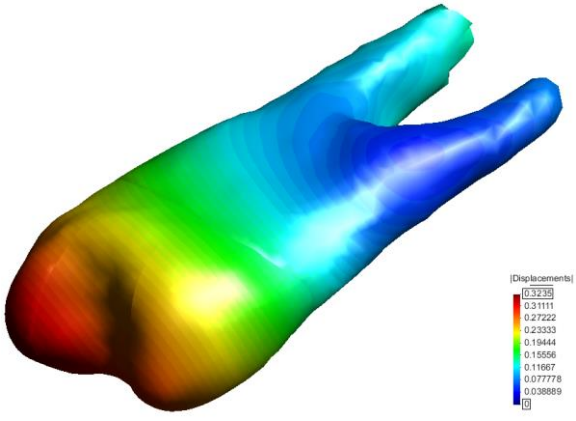

(d) GiD model solved in Matlab code, distal view.

Figure 5.18. Total displacement distributions (mm) for 3D model in elastic analysis

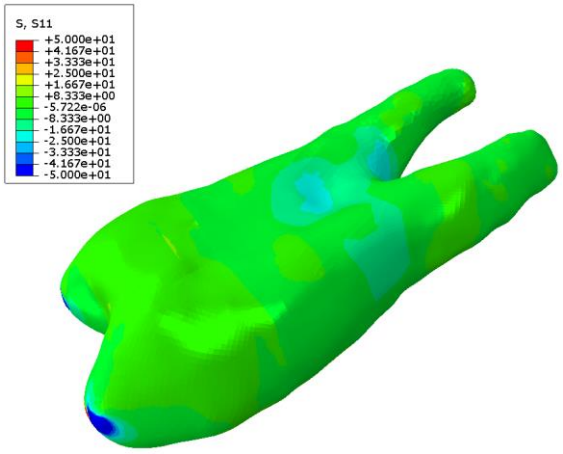

(a) Abaqus model, mesial view.

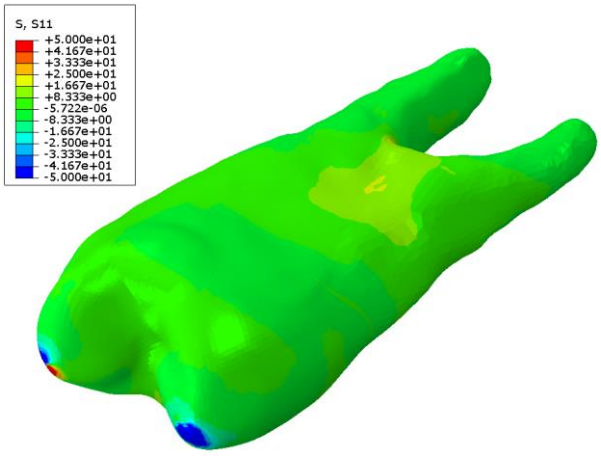

(b) Abaqus model, distal view.

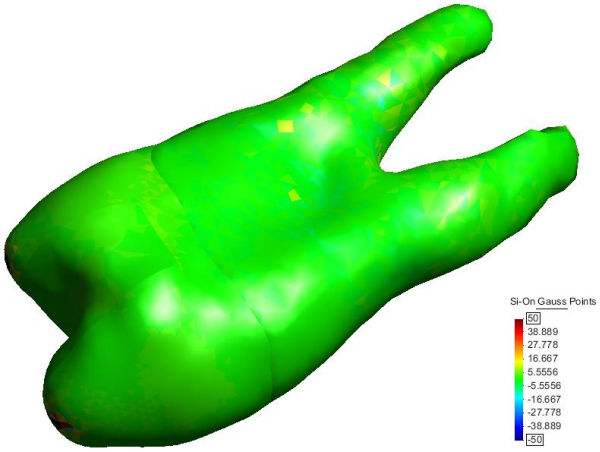

(c) GiD model solved in Matlab code, mesial view.

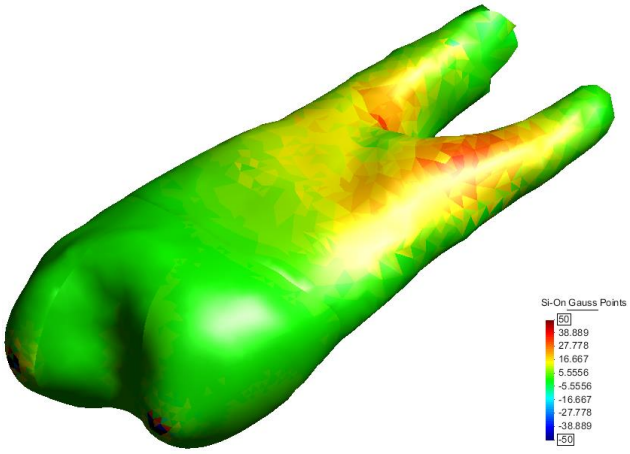

(d) GiD model solved in Matlab code, distal view.

Figure 5.19. S1 stress distributions (MPa) for 3D model in elastic analysis

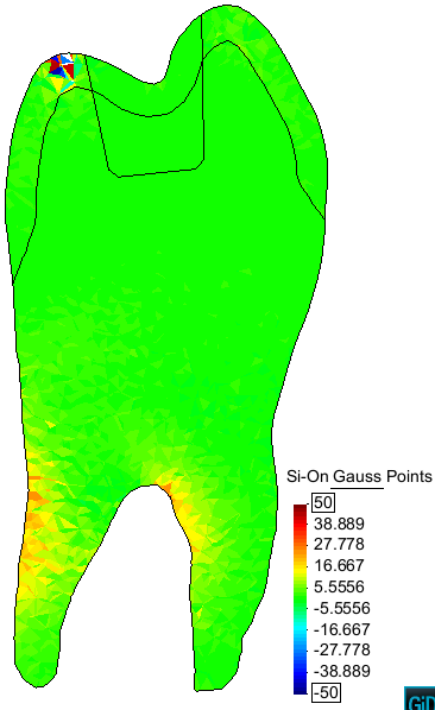

(a)

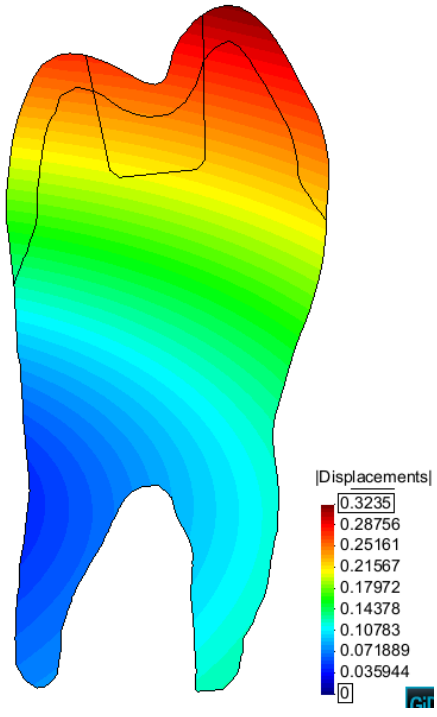

(b)

Figure 5.20. Section cut-plane for (a) S1 stress distributions (MPa), (b) Total displacement distributions (mm).

5.3 Concluding remarks

This thesis presented an elastic as well as fracture analyses of a premolar tooth under various loading conditions. The fracture modeling was done using the mesh fragmentation technique and crack propagation paths under various loading conditions were shown and analyzed. This technique was described in detail and the whole steps for conduct this study were brought and discussed. Here are the main conclusions from this thesis:

- It is very important to find whether the sane tooth can be broken under typical loadings.
- The results indicate that restored tooth in question did not reach critical stresses under usual mastication loads. Although, with the tensile strength of 32 MPa for dentin, there were some meaningful crack propagation, but for a value of 70 MPa of tensile strength (which is an average value obtained from Table 3.1), there was no crack propagation until the loading magnitude of 600 N. The sane teeth are safe if the materials have the expected properties, no cracks or discontinuities are present and the loads remain within expected values.
- The pre-existence of small initial cracks, due to the restorative process, can nevertheless lead to critical crack propagation.
- The loading type also plays a very important role in the crack propagation driving force. As it was shown in this chapter, the lingual load lead to some crack propagation while the buccal load lead to very small crack propagation. In addition, the combination of these two loads lead to a meaningful crack propagation path.
- Another important issue is the loading magnitude, a parameter for which a large variation is possible.
- The material properties also play a very critical role here, as the interface elements behavior mainly depends on the material properties of the region of interest. Therefore, they must be selected/defined in such a way that provide useful and reliable results.

5.4 Future Works

Here are some possible future works that can be done based on the current study:

- This study only provided some initial 3D elastic analysis, as the whole fracture analyses were done using a 2D model. Thus, the first ongoing task can to perform a fracture analysis of the 3D tooth using the mesh fragmentation technique.

- Since for 3D model, the loading points are not in the same plane, as they were in 2D model, it is very important to define the critical points that can be considered in the 3D model for the load application.
- This study only considered the composite resin as the restoration material. It could be interesting to study other types of restoration material and their effect on the fracture analysis. Also, study of other cavity configurations, like cusp protection, is another possible future work.

REFERENCES

Abou-Rass M, Crack lines: the precursors of tooth fractures—their diagnosis and treatment, Quintessence International, 1983, 14, pp. 437–447.

Bader JD, Martin JA, Shugars DA, Incidence rates for complete cusp fracture, Community Dentistry and Oral Epidemiology, 2001, 29, pp. 346–353.

Baker MI, Eberhardt AW, Martin DM, Mcgwin G, Lemons JE, Bone properties surrounding hydroxyapatite-coated custom osseous integrated dental implants. Journal of Biomedical Materials Research Part B: Applied Biomaterials, 2010, 95(1), pp. 218-224.

Banerji S, Mehta SB, Millar BJ, Cracked tooth syndrome. Part 1: Etiology and diagnosis, British Dental Journal, 2010a, 208(10), pp. 459-463.

Banerji S, Mehta SB, Millar BJ, Cracked tooth syndrome. Part 2: Restorative options for the management of cracked tooth syndrome, British Dental Journal, 2010b, 208(11), pp. 503-514.

Bazant ZP, Oh B, Crack band theory for fracture of concrete, RILEM Materials and Structures, 1983, 16, pp. 155-177.

Braly RV, Maxwell EH, Potential for tooth fracture in restorative dentistry, Journal of Prosthetic Dentistry, 1981, 45(4), pp. 411-414.

Brynjulfsen A, Fristad I, Grevstad T, Hals-Kvinnsland I, Incompletely fractured teeth associated with diffuse longstanding orofacial pain: diagnosis and treatment outcome, International Endodontic Journal, 2002, 35, pp. 461–466.

Cameron CE, Cracked-tooth syndrome, Journal of the American Dental Association, 1964, 68, pp. 405-11.

Cameron CE, The cracked tooth syndrome: additional findings, Journal of the American Dental Association, 1976, 93, pp. 971–975.

Cavel WT, Kelsey WP, Blankenau RJ, An in vivo study of cuspal fracture, Journal of Prosthetic Dentistry, 1985, 53, pp. 38–42.

Cervera M, Oliver J, Manzoli OL, A rate-dependent isotropic damage model for the seismic analysis of concrete dams. Earthquake Engineering and Structural Dynamics, 1996, 25(9), pp.987–1010.

Chung SM, Yap AU, Koh WK, Tsai KT, Lim CT, Measurement of Poisson's ratio of dental composite restorative materials. Biomaterials, Oxford, 2004, 25(13), pp. 2455-2460.

Cornacchia TPM, Las Casas EB, Cimini CA, Peixoto RG, 3D finite element analysis on esthetic indirect dental restorations under thermal and mechanical loading, Medical & Biological Engineering & Computing, 2010, 48, pp. 1107–1113.

Eakle WS, Maxwell EH, Braly BV, Fractures of posterior teeth in adults, Journal of the American Dental Association, 1986, 112, pp. 215–218.

Ellis SG, Incomplete tooth fracture — proposal for a new definition, British Dental Journal, 2001, 190(8), pp. 424-428.

Ellis SG, Macfarlane TV, McCord JF, Influence of patient age on the nature of tooth fracture, Journal of Prosthetic Dentistry, 1999, 82(2), pp. 226-230.

El Mowafy OM, Watts DC, Fracture toughness of human dentin, Journal of Dental Research, 1986, 65(5), pp. 677-681.

Ferrari EMM, Hickel R, Ilie N, Evaluation of the mechanical properties of dental adhesives and glass-ionomer cements, Clinical Oral Investigations, 2010, 14(1), pp. 79-87.

Filtek ™ Z250 Universal Restorative System - Technical Product Profile. Retrieved jan 28, 2014, from http://multimedia.3m.com/mws/mediawebserver?mwsId=66666UgxGCuNyXTtO8TXmX46EVtQEcuZgVs6EVs6E666666--&fn=Z250%20Tech%20Profile.pdf.

GiD - The personal pre and post processor, https://www.gidhome.com/, 2016.

Griffith AA, The phenomena of rupture and flow in solids, Philosophical Transactions of the Royal Society of London, A, 1921, 221, pp. 163–198.

Hamouda IM, Shehata SH, Fracture resistance of posterior teeth restored with modern restorative materials, Journal of Biomedical Research, 2011, 25(6), pp. 418-424.

Hiatt WH, Incomplete crown-root fracture in pulpal-periodontal disease, Journal of Periodontol, 1973, 44(6), pp. 369-379.

Hisam MJ, Lim JY, Kurniawan D, Nor FM, Stress Distribution due to Loading on Premolar Teeth Implant: A Three Dimensional Finite Element Analysis, Procedia Manufacturing, 2015, 2, pp. 218 – 223.

Hughes TJR, The Finite Element Method: Linear Static and Dynamic Finite Element Analysis, Dover, New York, 2000.

http://dentalcarematters.com/cracked-tooth/, last visited: January 2016.

Ingraea AR, Saouma V, Numerical modelling of discrete crack propagation in reinforced and plain concrete, In Fracture Mechanics of Concrete, Martinus Nijho Publishers, Dordrecht, 1985, pp. 171-225.

Irwin G, Analysis of stresses and strains near the end of a crack traversing a plate, Journal of Applied Mechanics, 1957, 24, pp. 361–364.

Kachanov LM, Introduction to continuum damage mechanics, Springer, Netherlands, 1986.

Kahler B, Swaina MV, Mouleb A, Fracture-toughening mechanisms responsible for differences in work to fracture of hydrated and dehydrated dentine. J. Biomech., v. 36, n. 2, p. 229-237, 2003.

Kinney JH, Balooch M, Marshall GV, A micromechanics model of the elastic properties of human dentine, Archives of Oral Biology, 1999, 44(10), pp. 813-822.

Kolmar W, Mehlhorn G, Comparison of shear stiffness formulations for cracked reinforced concrete elements, In: F. Damjanic et al., editors, Proceedings of International Conference on Computer Aided Analysis and Design of Concrete Structures, Part 1, Swansea, Pineridge Press, 1984, pp. 133-147.

Komatsu K, Mechanical Strength and Viscoelastic Response of the Periodontal Ligament in Relation to Structure, Journal of Dental Biomechanics, 2010, pp. 1-18.

Krell KV, Rivera EM, A six year evaluation of cracked teeth diagnosed with reversible pulpitis: treatment and prognosis, Journal Endodontic, 2007, 33, pp. 1405–1407.

Lagouvardos P, Sourai P, Douvitsas G, Coronal fractures in posterior teeth, Operations in Dentistry, 1989, 14, pp. 28–32.

Las Casas EB, Manzoli OL, Mattos CMA, Crack propagation in post-core rehabilitation of a maxillary central incisor after root reconstruction, Blucher Mechanical Engineering Proceedings, 2014, 1(1), pp. 1-11.

Lemaitre J, A course on damage mechanics, Springer, Netherlands, 1992.

Lin CL, Chang YH, Hsieh SK, Chang WJ, Estimation of the Failure Risk of a Maxillary Premolar with Different Crack Depths with Endodontic Treatment by Computer-aided Design/Computer-aided Manufacturing Ceramic Restorations, Journal of Endodontics, 2013, 39(3), pp. 375-379.

Lin CP, Cheng JH, Versluis A, Douglas WH, Failure criteria of dentin-resin adhesion—a mixed mode fracture mechanics approach, Scripta Materialia, 2000, 42(4), pp. 327–333.

Litonjua LA, Andreana S, Patra AK, Cohen RE, An assessment of stress analyses in the theory of abfraction, Bio-Medical Materials and Engineering, 2004, 14, pp. 311-321.

Lubisich EB, Hilton TJ, Ferracane J, Cracked teeth: a review of the literature, 2010, 22(3), pp. 158-167.

Lynch CD, McConnell RJ, The Cracked Tooth Syndrome, Journal of the Canadian Dental Association, 2002, 68 (6), pp. 470-475.

Lyons MF, Cadden SW, Baxendale RH, Yemm R, Twitch interpolation in the assessment of the maximum force-generating capacity of the jaw-closing muscles in man, Archives of Oral Biology, 1996, 41, pp. 1161-1168.

Manzoli OL, Gamino AL, Rodrigues EA, Claro GKS, Modeling of interfaces in two dimensional problems using solid finite elements with high aspect ratio, Computers and Structures, 2012, 94-95, pp. 70–82.

Manzoli OL, Maedo MA, Bitencourt LAG, Rodrigues EA, On the use of finite elements with a high aspect ratio for modeling cracks in quasi- brittle materials, Engineering fracture mechanic, 2016, 153, pp. 151-170.

Mattos CMA, Las Casas EB, Dutra IG, Sousa HA, Guerra SM, Numerical analysis of the biomechanical behaviour of a weakened root after adhesive reconstruction and post-core rehabilitation, Journal of Dentistry, 2012, 40, pp. 423-432.

Miguez PA, Pereira PN, Atsawasuwan P, Yamauchi M, Collagen cross-linking and ultimate tensile strength in dentin, Journal of Dental Research, 2004, 83(10), pp. 807-810.

Misch CE, Dental Implant Prosthetics, 2nd edition, Elsevier, The Netherlands, 2015.

Misch CE, Qu Z, Bidez MW, Mechanical properties of trabecular bone in the human mandible Implications for dental implant treatment planning and surgical placement, Journal of Oral and Maxillofacial Surgery, 1999, 57, pp. 700-706.

Munari LS, Cornacchia TMP, Moreira AN, Gonçalves JB, Las Casas EB, Magalhães CS, Stress distribution in a premolar 3D model with anisotropic and isotropic enamel, Medical and Biological Engineering and Computing, 2015, 53(8), pp. 751-758.

Murakami S, Continuum damage mechanics – a continuum mechanics approach to the analysis of damage and fracture, Springer, Netherlands, 2012.

Palamara JEA, Palamara D, Messer HH, Strains in the marginal ridge during occlusal loading, Australian Dental Journal, 2002, 47(3), pp. 218-222.

Phrukkanon S, Burrow MF, Tyas MJ, The effect of dentine location and tubule orientation on the bond strengths between resin and dentine, Journal of Dentistry, 1999, 27(4), pp. 265-274.

Pietrzak G, Curnier A, Botsis J, Scherrer S, Wiskott A, Belser U, A nonlinear elastic model of the periodontal ligament and its numerical calibration for the study of tooth mobility, Computer Methods in Biomechanics and Biomedical Engineering, 2002, 5(2), pp. 91-100.

Pokluda J, Andrea P, Micromechanisms of Fracture and Fatigue - In a Multi-scale Context, Springer-Verlag London, 2010.

Proesche PA, Morneburg T, Task-dependence of activity/bite force relations and its impact on estimation of chewing force from EMG, Journal of Dental Research, 2002, 81, 464-8.

Rashid YR, Analysis of prestressed concrete pressure vessels, Nuclear Engineering and Design, 1968, 7, pp. 334-344.

Reilly DT, Burstein AH, Review article. The mechanical properties of cortical bone, Journal of bone and joint surgery. American volume, 1974, 56(5), pp. 1001-1022.

Roh BD, Lee YE, Analysis of 154 cases of teeth with cracks, Dental Traumatology, 2006, 22, pp. 118–123.

Rosen H, Cracked tooth syndrome. Journal of Prosthetic Dentistry, 1982, 47(1), pp. 36-43.

Silva GR, Silva NR, Soares PV, Costa AR, Fernandes-Neto AJ, Soares CJ, Influence of Different Load Application Devices on Fracture Resistance of Restored Premolars, Brazilian Dental Journal (2012) 23(5), pp. 484-489.

Siso SH, Hurmuzlu F, Turgut M, Altundasar E, Serper A, Er K, Fracture resistance of the buccal cusps of root filled maxillary premolar teeth restored with various techniques, International Endodontic Journal, 2007(40), pp. 161–168

Slutzky-Goldberg I, Slutzky H, Gorfil C, Smidt A, Restoration of Endodontically Treated Teeth Review and Treatment Recommendations, International Journal of Dentistry, 2009, pp. 1-9.

Snyder DE, The cracked-tooth syndrome and fractured posterior cusp, Oral Surgery, Oral Medicine, Oral Pathology, Oral Radiology,1976, 41(6), pp. 698-704.

Suidan M, Schnobrich WC, Finite element analysis of reinforced beams, ASCE Journal of Structural Division, 1973, 99, pp. 2109-2122.

Swenson DV, Ingraea AR, Modeling mixed-mode dynamic crack propagation using finite elements: Theory and applications, Computational Mechanics, 1988, 3(5), pp. 381-397.

Talim ST, Gohil KS, Management of coronal fractures of permanent posterior teeth, Journal of Prosthetic Dentistry, 1974, 31, pp. 172–178.s

Thomaidis S, Kakaboura A, Mueller WD, Zinelis S, Mechanical properties of contemporary composite resins and their interrelations. Dental Mater, 2013, 29, pp. e132–e141.

Türp JC, Gobetti JP, The cracked tooth syndrome: an elusive diagnosis, Journal of the American Dental Association, 1996, 127(10), pp. 1502-1507.

Van Staden RC, Guan H, Loo YC, Application of the finite element method in dental implant research. Computer Methods in Biomechanics and Biomedical Engineering, 2006, 9(4), pp. 257-270.

Yahyazadehfar M, Bajaj D, Arola DD, Hidden contributions of the enamel rods on the fracture resistance of human teeth, Acta Biomaterialia, 2013, 9(1), pp. 4806- 4814.

Yahyazadehfar M, Ivancik J, Majd H, An B, Zhang D, Arola DD, On the Mechanics of Fatigue and Fracture in Teeth, Applied Mechanics Reviews, 2014, 66, pp. 1-16.

Zienkiewicz OC, Taylor RL, Zhu JZ, The Finite Element Method, Elsevier, Burlington, MA, 6th edn., 2005.